Title:

Stem cell mitotic drive ensures asymmetric epigenetic inheritance

Authors: Rajesh Ranjan[1], Jonathan Snedeker[1] and Xin Chen[1,*]

Affiliations:

[1] Department of Biology, The Johns Hopkins University, Baltimore, MD 21218

* Correspondence to: Xin Chen, Ph.D., Department of Biology, 3400 North Charles Street, The Johns Hopkins University, Baltimore, MD 21218-2685, Tel: 410-516-4576, Fax: 410-516-5213, Email: xchen32@jhu.edu

One Sentence Summary:

During *Drosophila* male germline stem cell division, asymmetric sister centromeres communicate with spindle microtubule differentially and bias sister chromatid segregation.

SUMMARY

Through mitosis, one mother cell gives rise to two identical daughter cells. The mitotic spindle interacts with sister chromatids to ensure their equal partitioning. By inheriting the identical genetic information, a crucial question is how cells become different to fulfill distinct functions during development and homeostasis. The "strand-specific imprinting and selective chromatid segregation" and "silent sister chromatid" hypotheses propose that epigenetic differences at the sister centromeres contribute to biased sister chromatid attachment and segregation during mitosis. However, direct *in vivo* evidence has never been shown. Here we report that a stem cell-specific 'mitotic drive' ensures biased sister chromatid attachment and asymmetric epigenetic inheritance. We found that temporally asymmetric microtubule activities direct polarized nuclear envelope breakdown, allowing for the preferential recognition and attachment of sister centromeres with quantitative differences. This communication occurs in a spatiotemporally regulated manner to ensure selective attachment of sister chromatids by the mitotic machinery. Abolishment of the microtubule asymmetries result in randomized sister chromatid segregation. Our results demonstrate that the *cis*-asymmetry at chromatids tightly coincide and coordinate with the *trans*-asymmetry from the mitotic machinery, to allow for differential attachment and segregation of genetically identical but epigenetically distinct sister chromatids. Together these results provide the first direct *in vivo* evidence to support the above hypotheses in asymmetrically dividing stem cells. We anticipate that this 'mitotic drive' mechanism could be widely used in other developmental context to achieve distinct cell fates between the two genetically identical daughter cells.

INTRODUCTION

Epigenetic mechanisms play important roles in regulating stem cell identity and activity. Inappropriate regulation of epigenetic information may lead to abnormalities in stem cell behaviors that underlie early steps in diseases such as cancers and tissue degeneration. Since epigenetic mechanisms play a crucial role in regulating cell identity and behavior, the field has long sought to understand how stem cells maintain their epigenetic memory through many cell divisions. A major group of epigenetic information carriers are histone proteins, which have important contributions to DNA packaging and differential gene expression regulation.

Many types of adult stem cells undergo asymmetric cell division (ACD) to generate both a self-renewed stem cell and a daughter cell which will subsequently differentiate (Betschinger and Knoblich, 2004; Clevers, 2005; Inaba and Yamashita, 2012; Morrison and Kimble, 2006). During the asymmetric division of *Drosophila* male germline stem cells (GSCs) (Figure 1A), we previously showed that the preexisting (old) histone H3 is selectively segregated to the GSC, whereas the newly synthesized (new) H3 is enriched in the differentiating daughter cell known as a gonialblast (GB) (Tran et al., 2012). We also identified that differential phosphorylation at Threonine 3 of histone H3 (H3T3P) distinguishes old *versus* new H3 in asymmetrically dividing GSCs. Mis-regulation of this phosphorylation leads to randomized segregation of old *versus* new H3, as well as stem cell loss and early-stage germline tumor (Xie et al., 2015). We hypothesize that prior to mitosis, old and new H3 are differentially distributed at the two sets of sister chromatids (Wooten, 2018). During the subsequent mitosis, the two sets of epigenetically distinct sister chromatids are asymmetrically segregated (Tran et al., 2013; Xie et al., 2017). According to this model, sister chromatids carrying distinct epigenetic information need to communicate with the mitotic machinery to achieve differential attachment, followed by

asymmetric segregation. It has been shown previously that centrosomes display asymmetry in male GSCs wherein the mother centrosome is retained by the GSC while the daughter centrosome is inherited by the GB (Yamashita et al., 2007). However, it remains unclear whether this asymmetry in centrosome inheritance may be related to the phenomenon of asymmetric histone inheritance.

During mitosis, microtubules nucleate from centrosomes and attach to sister chromatids at the centromeric region. The centromere, which represents a specialized region of the chromosome (Dunleavy et al., 2005), serves as an assembly platform for attachment and segregation of sister chromatids by microtubules (Westhorpe and Straight, 2014). Based on the unique features and essential roles of the centromere in mitosis, it has been proposed that epigenetic differences between sister centromeres could ensure that stem cells retain their unique epigenetic information and gene expression through many cell divisions (Lansdorp, 2007). Centromeres are epigenetically defined in most eukaryotes by a centromere-specific histone H3 variant known as Centromere identifier (CID) in flies and CENP-A in mammals (Allshire and Karpen, 2008; Palmer et al., 1987), each of which are structurally different from the canonical H3 (McKinley and Cheeseman, 2016; Miell et al., 2013). Here we report an axis of spatiotemporally controlled asymmetry in *Drosophila* male GSCs from sister centromeres, relayed to sister kinetochores and recognized by temporally asymmetric microtubule activity. Our results shed light on the cellular basis underlying how genetically identical but epigenetically distinct sister chromatids are recognized and segregated by the mitotic machinery in asymmetrically dividing stem cells.

RESULTS

Asymmetric Sister Centromere Inheritance in Male GSCs

During *Drosophila* male GSC asymmetric division, the level of endogenous CID showed a 1.41-fold enrichment at sister chromatids segregating toward the future GSC side compared to the future GB side in anaphase and early telophase GSCs, examined by immunostaining using anti-CID antibodies (Figures 1B and 1D, Figures S1A and S1C). Conversely, symmetrically dividing spermatogonial cells (SGs) showed symmetric CID distribution in anaphase and early telophase SGs (Figures 1C and 1D, Figures S1B and S1D). To further validate this result, live cell imaging was performed using a knock-in fly strain with the endogenous *cid* gene tagged with a fluorescent protein-encoding *Dendra2* (Chudakov et al., 2007), which was generated by CRISPR/Cas9-mediated genome editing (Horvath and Barrangou, 2010; Wright et al., 2016). Consistent with the immunostaining results, CID-Dendra2 also displayed a 1.39-fold overall enrichment at sister chromatids segregating toward the future GSC side compared to the future GB side (Figures 1D and 1E, Movie S1). Additionally, CID-Dendra2 showed symmetric distribution patterns in SGs (Figures 1D and 1F, Movie S2). Finally, a CID-GFP genomic transgene used in previous studies (Henikoff et al., 2000) showed a 1.73-fold enrichment toward the future GSC side compared to the future GB side in asymmetrically dividing GSCs (Figures S1E and S1G, Movie S3). By contrast, symmetric distribution of CID-GFP was found in symmetrically dividing SGs (Figures S1F and S1G, Movie S4). Together, both endogenous and transgenic CID showed enrichment toward the future stem cell side during GSC asymmetric division, using both immunostaining on fixed samples and live cell imaging.

We hypothesize that the overall asymmetric CID segregation could be due to asymmetry at individual pairs of sister centromeres. To test this hypothesis, we examined sister centromeres

before their segregation in anaphase or telophase. Indeed, in metaphase GSCs, the individual sister centromere with more CID signals was oriented toward the future GSC side (Figure 1G), suggesting that the stronger sister centromere was preferentially recognized by the mother centrosome-emanating microtubules. Again, this asymmetry of individual sister centromere was not detected in metaphase SG (Figure 1H). Furthermore, in GSCs at prophase to prometaphase when centromeres exhibit dynamic crosstalk with the mitotic spindle microtubules, sister centromeres that could be resolved at this stage already displayed a level of quantitative difference in that one sister centromere displayed on average a 1.52-fold more CID compared to the other sister centromere (Figure 1I, Figures S1H, S2A-D). On the other hand, all sister centromeres resolved in SGs showed no obvious difference (Figures 1I, Figures S1I, S2A-D). In summary, the sister centromere with more CID is oriented and segregated to the future stem cell side in asymmetrically dividing GSCs (Figures 1B, 1E, S1C, S1E, S2E) but not in symmetrically dividing SGs (Figures 1C, 1F, S1D, S1F, S2F). Notably, not all sister centromeres were resolved at the same time in GSCs. The earlier resolved sister centromeres displayed a higher degree of asymmetry compared to those resolved later, resulting in two groups of sister centromeres with different degrees of asymmetry (Figure 1I, sister centromeres labeled with red bracket showed more asymmetry than those labeled by magenta bracket). The sequentially resolved sister centromeres could be regulated temporally or in a chromosome-specific manner, or both.

Asymmetric Kinetochore Acts as a Relay of the Asymmetry between Sister Centromeres in GSCs

The recognition of centromeres by microtubules is mediated by the kinetochore, a highly organized multiprotein structure which nucleates at the surface of centromere and coordinates the

attachment of the mitotic spindle (Cheeseman, 2014; Cleveland et al., 2003). We next examined a kinetochore protein, NDC80, using a *Dendra2-Ndc80* knock-in fly strain. Consistent with the asymmetry of CID, the kinetochore component NDC80 displayed a 1.49-fold overall enrichment at sister chromatids segregated toward the future GSC side in anaphase and early telophase GSCs (Figures 2A and 2C). In contrast, symmetrically dividing SGs displayed a symmetric NDC80 segregation pattern (Figures 2B and 2C). Moreover, differences between sister kinetochores were already detectable in prometaphase GSCs (Figure 2D), but not in prometaphase SGs (Figure 2E). Individual pairs of sister kinetochores showed, on average, a 1.76-fold difference in prometaphase GSCs (Figure 2F). However, no obvious difference among sister kinetochores could be detected in prometaphase SGs (Figure 2F). Noticeably, sister kinetochore asymmetry showed the same enrichment compared to sister centromeres (Figure 2D), but was quantitatively greater than the sister centromere asymmetry (Figures 2D and 2G), suggesting a possible 'relay' mechanism enabling the kinetochore to recognize the centromere difference and amplify it. Furthermore, the sister kinetochore with more NDC80 signal was oriented toward the future GSC side in metaphase GSCs (Figures 2H and S3A), whereas symmetric NDC80 between each pair of sister kinetochores was detected in metaphase SGs (Figures 2I and S3B). Collectively, these results demonstrate that sister centromeres and sister kinetochores are quantitatively different in mitotic GSCs, differentially preparing sister chromatids for asymmetric attachment. Together with the asymmetric phosphorylation of H3T3, sister centromeres and kinetochores likely serve as *cis*-mechanisms for differential recognition and attachment of epigenetically different sister chromatids by the mitotic machinery in GSCs (Figure S3C).

Temporally Asymmetric Microtubule Dynamics in GSCs

To understand how *cis*-asymmetry on sister chromatids could be recognized by the mitotic spindle, we tracked microtubules using a GFP-tagged α-Tubulin under the control of an early-stage germline-specific *nanos-Gal4* driver (Van Doren et al., 1998). Using high temporal resolution movies, we tracked microtubules in real-time throughout the cell cycle of germ cells at distinct differentiation stages. Using metaphase as a landmark to define time point zero, other cell cycle phases were labeled by minutes prior to metaphase. In GSCs, from -250min (mid-G2 phase) to -150min (late-G2 phase), more microtubules nucleated from the mother centrosome than microtubules from the daughter centrosome (Figure 3A, Movie S5). Subsequently, this dominance of mother centrosome-nucleating microtubule declined from -50min to -35min (G2/M transition) as the daughter centrosome- nucleating microtubules increased (Figures 3A and 3C, Movie S5). This decrease of mother centrosome-nucleating microtubule and increase of daughter centrosome-nucleating microtubule persisted in GSCs from -30min to -10min (prophase) and at -5min (prometaphase) (Figures 3A and 3C, Movie S5). At 0min (metaphase), the mitotic spindle with overall comparable microtubules from both centrosomes formed in perpendicular to the GSC-niche interface (Figures 3A and 3C, Movie S5), as reported previously (Yamashita et al., 2003). Conversely, in SGs, microtubules from both centrosomes were detectable at -35min at the G2/M transition, and no obvious difference could be detected between the activity of the two centrosomes throughout mitosis (Figures 3B and 3D, Movie S6). In summary, these results demonstrate that the key component of the mitotic machinery, microtubules, display a temporal asymmetry in male GSCs.

Polarized Nuclear Envelope Breakdown Induced by Temporally Asymmetric Microtubules

Next, using high spatial resolution movies, we found that mother centrosome-emanating microtubules started 'poking in' the nuclear envelope from late G2 phase to early prophase in GSCs (Figure S4A, Movie S7). This dynamic activity of microtubules resulted in invagination of the nuclear lamina from the future stem cell side, as visualized by immunostaining using antibodies against *Drosophila* Lamin-B (Chen et al., 2013) (Figure 4A, Movie S8A-C). Local disassembly of nuclear lamina was first detected at the future stem cell side (green arrows in Figure 4A and Movie S8A-C). Subsequently, increased microtubule dynamics from the daughter centrosome led to invagination of nuclear lamina from the GB side (red arrowheads in Figure 4B and Movie S9A-B). This led to eventual nuclear envelope breakdown (NEBD). By contrast, such a sequential NEBD was not observed in symmetrically dividing SGs (yellow arrowheads in Figure 4C and yellow arrows in Figure 4D).

Similar results were obtained using wheat germ agglutinin (WGA) which binds to the cytoplasmic part of each nuclear pore, in order to visualize nuclear membrane morphology in GSCs (Figures 4E and 4F) and SGs (Figures 4G and 4H). Therefore, in GSCs the temporally asymmetric microtubule dynamics likely result in NEBD in a polarized manner, first at the GSC side and subsequently at the GB side.

Trans-Asymmetry of the Mitotic Machinery Coordinates with the *Cis*-Asymmetry of Sister Centromeres

We next asked whether the *trans*-asymmetry of microtubule and NEBD coincide and coordinate with the *cis*-asymmetry at sister centromeres in GSCs. Noticeably, in GSCs at late G2 phase, close proximity between chromosomes and microtubules could be detected: When mother centrosome-emanating microtubules dynamically interacted with the nuclear envelope (α-

Tubulin and Lamin in Figure 5A), centromeres from all chromosomes clustered preferentially toward the future GSC side (CID in Figure 5A, Figure S4B). Previously, the 'chromocenter' structure with clustered peri-centromeric chromosomal region was reported in interphase mouse (Hsu et al., 1971) and fly (Jagannathan et al., 2018) cells. Given the higher microtubule dynamics from the mother centrosome, this close proximity of all centromeres toward the future GSC side might initiate crosstalk between centromeres and mother centrosome-emanating microtubules.

At the G2/M transition, the more active microtubules from the mother centrosome (α-Tubulin in Figure 5B) led to deep invagination of the nuclear envelope toward the GSC side (Lamin in Figure 5B, green arrowhead). Meanwhile, clustered centromeres started to decluster but were still close to the nuclear envelope toward the GSC side (CID in Figure 5B). Once mitosis was initiated, microtubule activities from both centrosomes were detectable in early prophase GSCs (α-Tubulin in Figure 5C), when the mitotic chromosome marker H3S10P became more abundant in the nucleus (S10P in Figure 5C). The nuclear envelope showed polarized breakdown with the intact GB side but broken GSC side (Lamin in Figure 5C, green arrow). At this time, centromeres were de-clustered with some sister centromeres resolved and displayed asymmetric CID signals (CID in Figure 5C; inset showed a pair of resolved sister centromeres). This trend extended to late prophase when microtubules from the daughter centrosome were more active (α-Tubulin in Figure 5D) and condensed chromosomal morphology was visible with the intensive H3S10P signal (S10P in Figure 5D). At prometaphase, the mitotic spindle formed (α-Tubulin in Figure 5E), even though the nuclear lamina was still maintained to a certain degree (Lamin in Figure 5E), similar to a phenomenon previously reported in *Drosophila* embryos (Debec and Marcaillou, 1997; Kiseleva et al., 2001;

Stafstrom and Staehelin, 1984). At anaphase, sister chromatids were segregated and clear CID asymmetry was observed between the two sets of sister centromeres [CID in Figure 5F, enlarged panels show the set of centromeres segregated to the future GSC side (outlined by green dotted line) *versus* the ones segregated to the future GB side (outlined by red dotted line)]. Together, this series of immunostaining images with markers for both the *trans*-factors, such as microtubule and nuclear lamina, and the *cis*-factors of CID at sister centromeres depicted a sequential order of their dynamic interactions from late G2 phase to anaphase, through which the stronger centromere with more CID is preferentially recognized by the early active mother-centrosome nucleating microtubules (Figure S4C).

Next, we examined these events in symmetrically dividing SG cells: Even though microtubule activity (α-Tubulin in Figure S5B) still coincided with chromosomal condensation (S10P in Figure S5B-E) and centromere movement (CID in Figure S5B-E), no obvious sequential order was observed for microtubules emanating from both centrosomes and no detectable asymmetry was found between resolved individual pairs of sister centromeres (CID in inset at late prophase in Figure S5C). Consistently, at anaphase the overall CID signals between the segregated two sets of sister chromatids were also symmetric (CID in Figure S5F).

To investigate whether the *trans*-asymmetry of microtubule leads to differential sister chromatid attachment more directly, we used cold treatment to stabilize microtubules especially the Kinetochore fibers (K-fibers) (Akera et al., 2017; Rieder, 1981). We then performed immunostaining of sister centromeres followed by high spatial resolution imaging. We found in metaphase GSCs, the stronger sister centromere was attached by the mother centrosome emanating K-fibers, while the weaker centromere was attached by the daughter centrosome-emanating K-fibers (α-Tubulin and CID in Figure 1G and Figure S5A). Taken together,

temporally asymmetric microtubules coordinate with quantitatively asymmetric sister centromeres and sister kinetochores, in order to ensure differential sister chromatid attachment followed by asymmetric segregation (Figure 5G), consistent with what has been previously hypothesized (Kahney et al., 2018; Malik, 2009; Yamashita, 2013).

Depolymerizing Microtubule Disrupts the *trans* Asymmetry of the Mitotic Machinery

To investigate the regulation of the sequential asymmetric microtubules in GSCs, we need a method to acutely disrupt this asymmetry without affecting the overall germline fitness. To accomplish this, we designed a regime using the microtubule depolymerizing drug Nocodazole (NZ) on testes *ex vivo*, followed by washout and immunostaining (Figure 6A). GSCs treated with NZ were arrested at the G2/M transition, but following washout, they were released and progressed through mitosis in a time-dependent manner (Figures 6A and S6A). After washing out NZ and allowing time for recovery, GSCs displayed symmetric microtubule dynamics, suggesting that the temporal asymmetry of microtubules could be disrupted under this condition (Figures 6B, 6C and S6B).

Next, we examined NEBD in GSC and SG after releasing from NZ treatment. The sequential invagination and disassembly of nuclear lamina observed in GSCs (Figures 4A-B, 5B-E) became undetectable: both mother and daughter centrosomes showed similar microtubule-emanating activity (green and red arrowheads for α-Tubulin signal in Figure 6D), and no obvious dominant side of 'poking in' activity was observed (green and red arrowheads for Lamin signal in Figure 6D). At prometaphase, NEBD occurred from both sides (green and red arrows for Lamin signal in Figure 6E), coinciding with comparable microtubules from both centrosomes (green and red arrows for α-Tubulin signal in Figure 6E). These events in GSCs resembled the

microtubule dynamics and NEBD events in SGs (yellow arrowheads in Figure 6F and yellow arrows in Figure 6G). Noticeably, in GSCs the centrosomes were already duplicated and well oriented in perpendicular to the GSC-niche interface at early prophase (green and red arrowheads for α-Tubulin signal in Figure 6D). This observation is consistent with the previous report that centrosomes are duplicated and migrated during G2 phase (Yamashita et al., 2003), which also confirms that the treatment with NZ followed by release changed microtubule emanation in an acute manner since the centrosome duplication and migration were not disrupted.

Disruption of the Temporal Asymmetry of Microtubules Leads to Abnormal Centromere and Histone Inheritance Patterns in GSCs

To determine whether the temporally asymmetric microtubules are, in fact, necessary for asymmetric sister chromatid segregation, we applied the NZ treatment followed by washout and immunostaining regime, as described above (Figure 6A). Under this condition, asymmetric sister centromere segregation was also lost, as visualized by anti-CID immunostaining at anaphase and early telophase (Figures 7A and 7B), suggesting that sister chromatids had been randomly segregated following the loss of temporal asymmetry of microtubule dynamics.

Consistently, when we examined the segregation pattern of old *versus* new histone H3 in anaphase or telophase mitotic GSCs recovered from NZ treatment, both displayed symmetric patterns (Figures 7C and 7D). Abnormal H3 and CID inheritance patterns suggest that the asymmetric sister chromatid inheritance is abolished when temporal asymmetry of microtubule dynamics is disrupted. In conclusion, these results indicate that the *trans*-asymmetry from the mitotic machinery is required for *cis*-elements at sister chromatids, such as CID and H3, to be recognized and properly segregated (Figure S6C).

Discussion

Here we have shown that asymmetrically dividing GSCs utilize a cohort of *trans*- and *cis*-factors to recognize and segregate epigenetically distinct sister chromatids. The previously identified asymmetrically inherited centrosomes (Yamashita et al., 2007), the herein reported temporally asymmetric microtubules, and polarized NEBD all serve as an axis of asymmetric *trans*-factors within the mitotic machinery. Meanwhile, the previously identified asymmetric H3 (Tran et al., 2012), the differential phosphorylation at Thr3 of H3 (Xie et al., 2015), and the herein reported asymmetric sister centromeres and kinetochores act as a series of *cis*-factors. Together the *trans*-factors coordinate and recognize the distinct *cis*-factors between sister chromatids for their proper attachment and segregation in order to generate two epigenetically distinct daughter cells (Figure 5G). Together, asymmetric epigenetic inheritance pattern is achieved during *Drosophila* male GSC division, which in turn supports our hypothesis of a 'mitotic drive'.

The ACD gives rise to two daughter cells with distinct fates, which occurs widely during development, tissue homeostasis, and regeneration (Betschinger and Knoblich, 2004; Clevers, 2005; Inaba and Yamashita, 2012; Morrison and Kimble, 2006). It is conceivable that the centromere and kinetochore asymmetry may provide molecular mechanisms for selective sister chromatid segregation during ACD (Yadlapalli and Yamashita, 2013). Previously, two similar models, named the "strand-specific imprinting and selective chromatid segregation"(Klar, 1994, 2007) and "silent sister chromatid" (Lansdorp, 2007), suggest that epigenetic differences between sister chromatids, especially at the centromere region, are required to direct the asymmetric outcomes during ACD. However, up to date no clear evidence supporting these

hypotheses has been shown. Here our findings not only provide the first direct *in vivo* evidence in support of these hypotheses, but also reveal detailed cellular bases and consequences of disrupting them in changing biased sister chromatid segregation.

Previously, a phenomenon called "meiotic drive" has been proposed, in which the allele with a stronger kinetochore is retained in the oocyte while the allele with a weaker kinetochore is segregated to polar bodies during meiosis (Pardo-Manuel de Villena and Sapienza, 2001a, b). Recently, it has been shown that during this selection process in female mice, the stronger kinetochore often associates with the longer "selfish" centromere and has more affinity to the meiotic spindle, which itself has been asymmetrically modified due to polarized signaling (Akera et al., 2017; Chmatal et al., 2014; Iwata-Otsubo et al., 2017; Kursel and Malik, 2018). Additionally, it has also been shown that a microtubule motor protein regulates meiotic drive in maize, indicating a role of microtubules in selective attachment to centromeres in this system (Dawe et al., 2018; Schroeder and Malik, 2018).

However, it is unclear whether these asymmetric functions of kinetochore and centromere could act in mitosis and regulate sister chromatid segregation. Here our results reveal that a similar mechanism may also exist in mitosis. Nevertheless, the 'mitotic drive' has distinct features compared with the 'meiotic drive'. First, in meiosis the centromere difference occurs between specific homologous chromosomes, whereas in mitosis it occurs between genetically identical sister chromatids. Second, in meiosis the microtubule itself does not have any temporally asymmetric activity but has different modifications instead. By contrast, in mitosis different amount of microtubules emanate from either mother centrosome or daughter centrosome, which could be visualized in a sequential order. Third, the biological outcome is different: the 'meiotic drive' leads to retention of the particular allele with stronger kinetochore

and "selfish" centromere to the haploid oocyte, whereas the 'mitotic drive' leads to two diploid cells with distinct epigenetic information.

In summary our results demonstrate that the *cis*-asymmetry at sister chromatids tightly coincide and coordinate with the *trans*-asymmetry from the mitotic machinery. Together, this spatiotemporally regulated axis of asymmetry, i.e. sister centromeres → sister kinetochores → nuclear membrane→ microtubules, allows for differential attachment and segregation of epigenetically distinct sister chromatids. Our studies provide direct *in vivo* evidence to support the "strand-specific imprinting and selective chromatid segregation" and the "silent sister chromatid" hypotheses in asymmetrically dividing stem cells. Together, our discovery helps understanding of a fundamental question in biology regarding how mitotic machinery could distinguish and ensure asymmetric partitioning of epigenetic information, which could be widely utilized in other context of multicellular organisms to generate cells with distinct fates.

Figures and Figure Legends:

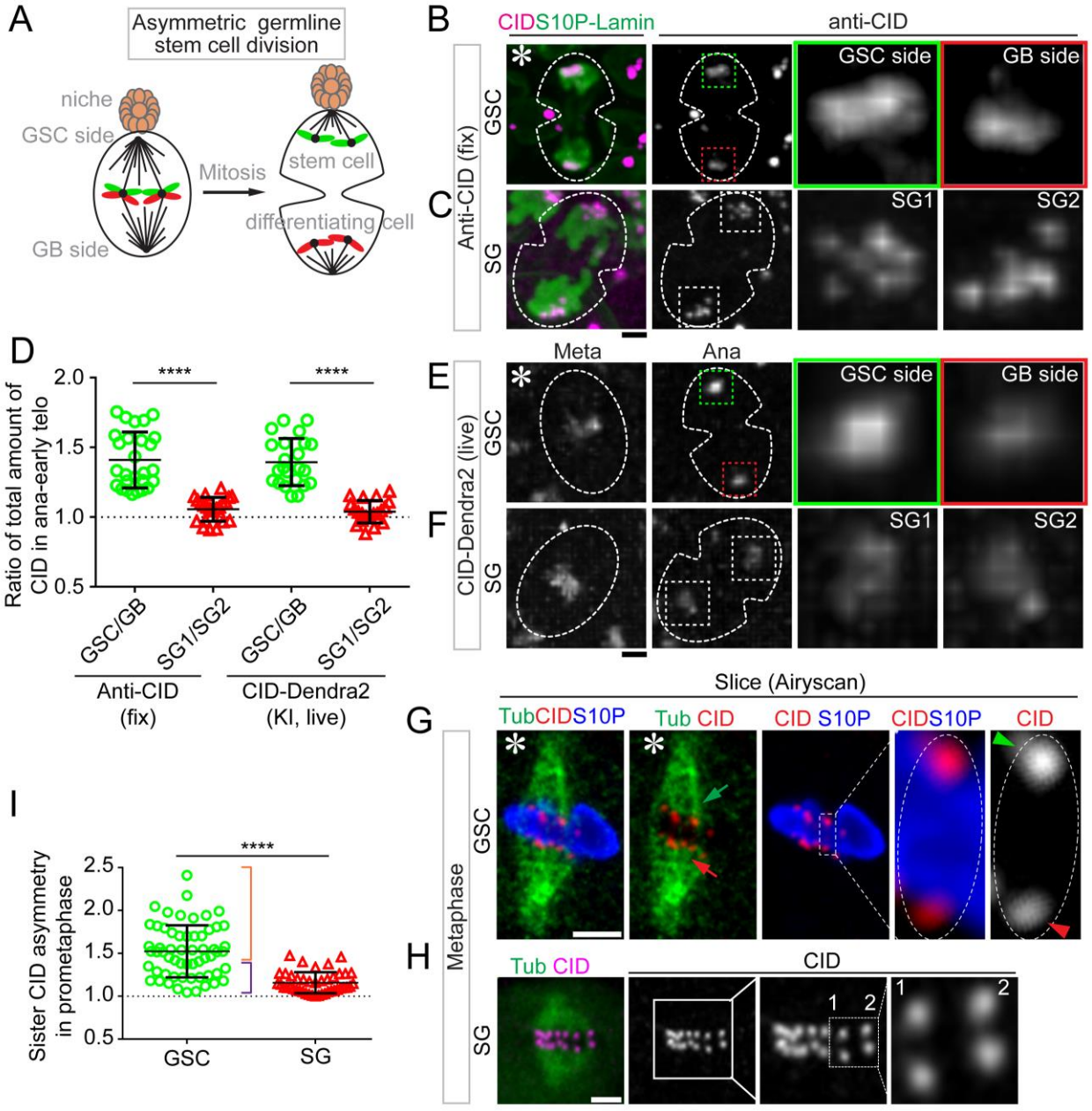

Figure 1: Asymmetric CID inheritance in GSCs. (**A**) A cartoon depicting asymmetric *Drosophila* male GSC division and asymmetric histone H3 inheritance (old H3 -green, new H3 -red). (**B-F**) Asymmetric CID segregation in asymmetrically dividing GSCs with more CID toward the GSC side, using both immunostaining of fixed cells (**B**) and live cell imaging of a CID-Dendra2 knock-in line (**E**). In symmetric SG cell division, CID is symmetrically

distributed, as determined using both immunostaining (**C**) and live cell imaging (**F**). Quantification of all four data sets in (**D**): 1.41± 0.20-fold for GSC/GB (*n*= 27), 1.06± 0.90-fold for SG1/SG2 (*n*= 23), as determined by anti-CID, Table S1; 1.39± 0.17-fold for GSC/GB (*n*= 23), 1.04± 0.08-fold for SG1/SG2 (*n*= 21), as determined by live cell imaging using CID-Dendra2, Table S2. (**G**) A metaphase GSC showing more substantial microtubule (green arrow) attachment to the stronger centromere (green arrowhead) toward the GSC side, compared to the microtubule (red arrow) attached to the weaker centromere (red arrowhead), co-stained with anti-H3S10P (blue). (**H**) Such a phenomenon was not detected in SGs. (**I**) Quantification of individual pairs of resolved sister centromeres in GSCs (*n*= 59) at prometaphase [1.52± 0.04-fold, red bracket indicates a more asymmetric group; 1.15± 0.02-fold in SGs (*n*= 43), Table S4]. All ratios= Avg± SE; *P*-value: paired *t* test. ****: $P< 10^{-4}$. Asterisk: hub. Scale bars: 2μm.

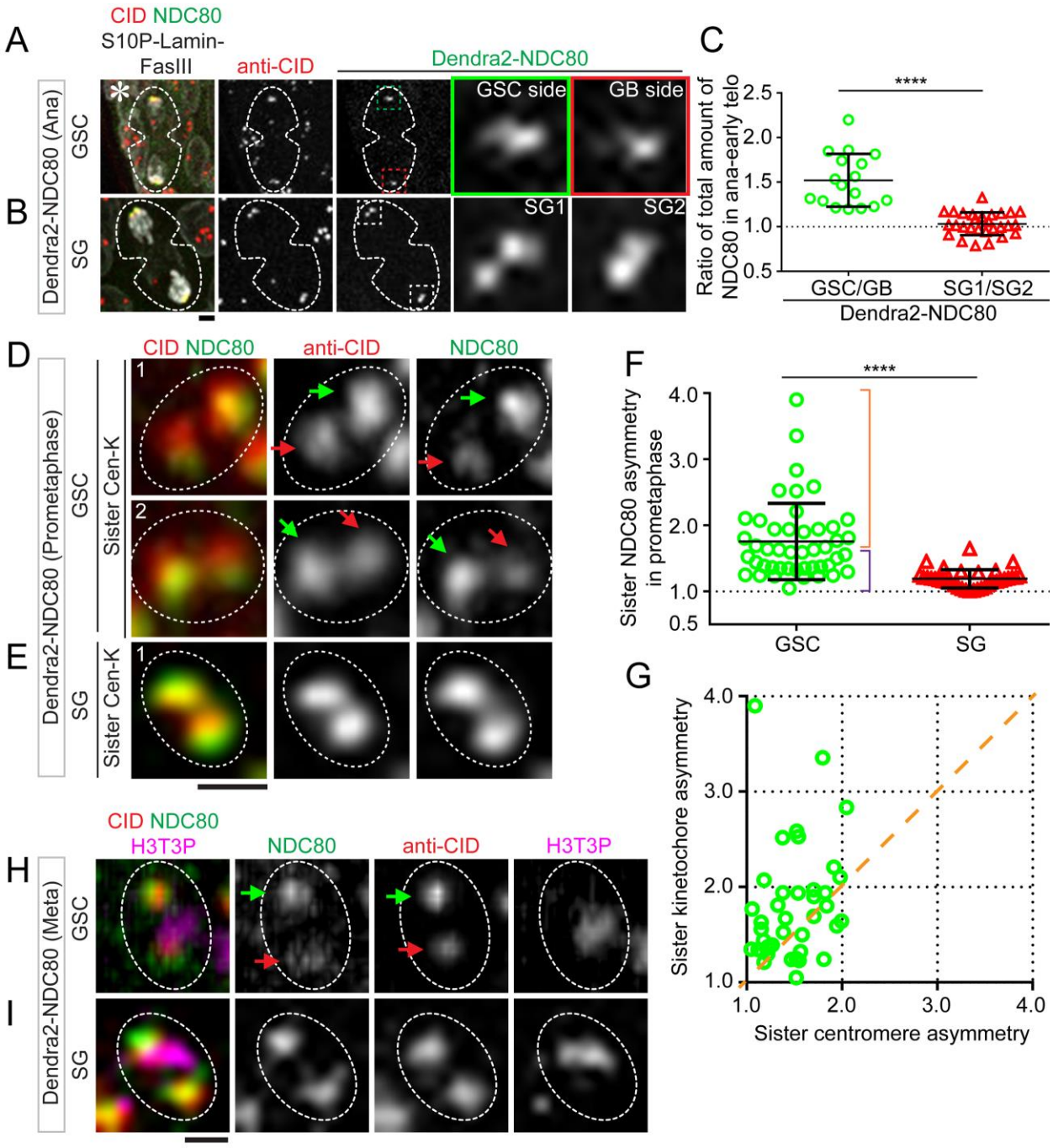

Figure 2: Asymmetric kinetochore relays the asymmetry of sister centromeres in GSCs. (**A**) Asymmetric kinetochore component NDC80 in asymmetrically dividing GSCs with more NDC80 toward the GSC side, using immunostaining of a Dendra2-NDC80 knock-in line. (**B**) In symmetric SG cell division, NDC80 is symmetrically distributed. (**C**) Quantification of both data

sets: GSC/GB= 1.49± 0.07 (*n*= 19), SG1/SG2= 1.03± 0.03 (*n*= 28), Table S5. (**D**-**E**) In prometaphase, resolved sister kinetochores show more asymmetry in GSCs (**D**), compared to resolved sister kinetochores in SGs (**E**). (**F**) Quantification of individual pairs of resolved sister kinetochores in prometaphase: 1.76± 0.08-fold in GSCs (*n*= 46), red bracket indicates a more asymmetric group; 1.19± 0.02-fold in SGs (*n*= 34), Table S6. (**G**) In prometaphase GSCs, asymmetric NDC80 is coupled with asymmetric CID. The degree of asymmetry for sister kinetochore is more than that for sister centromere, indicating the presence of a 'relay' mechanism [CID = 1.49-fold, NDC80 = 1.76-fold (*n*= 43), Table S7]. (**H**) At metaphase, the stronger NDC80 is coupled with stronger CID, which are oriented toward the GSC side. (**I**) Such a phenomenon was not detected in SGs. All ratios= Avg± SE; *P*-value: paired *t* test: ****: $P< 10^{-4}$, Asterisk: hub. Scale bars: 2μm (**A**-**B**) and 0.5μm (**D**-**E**, **H**-**I**).

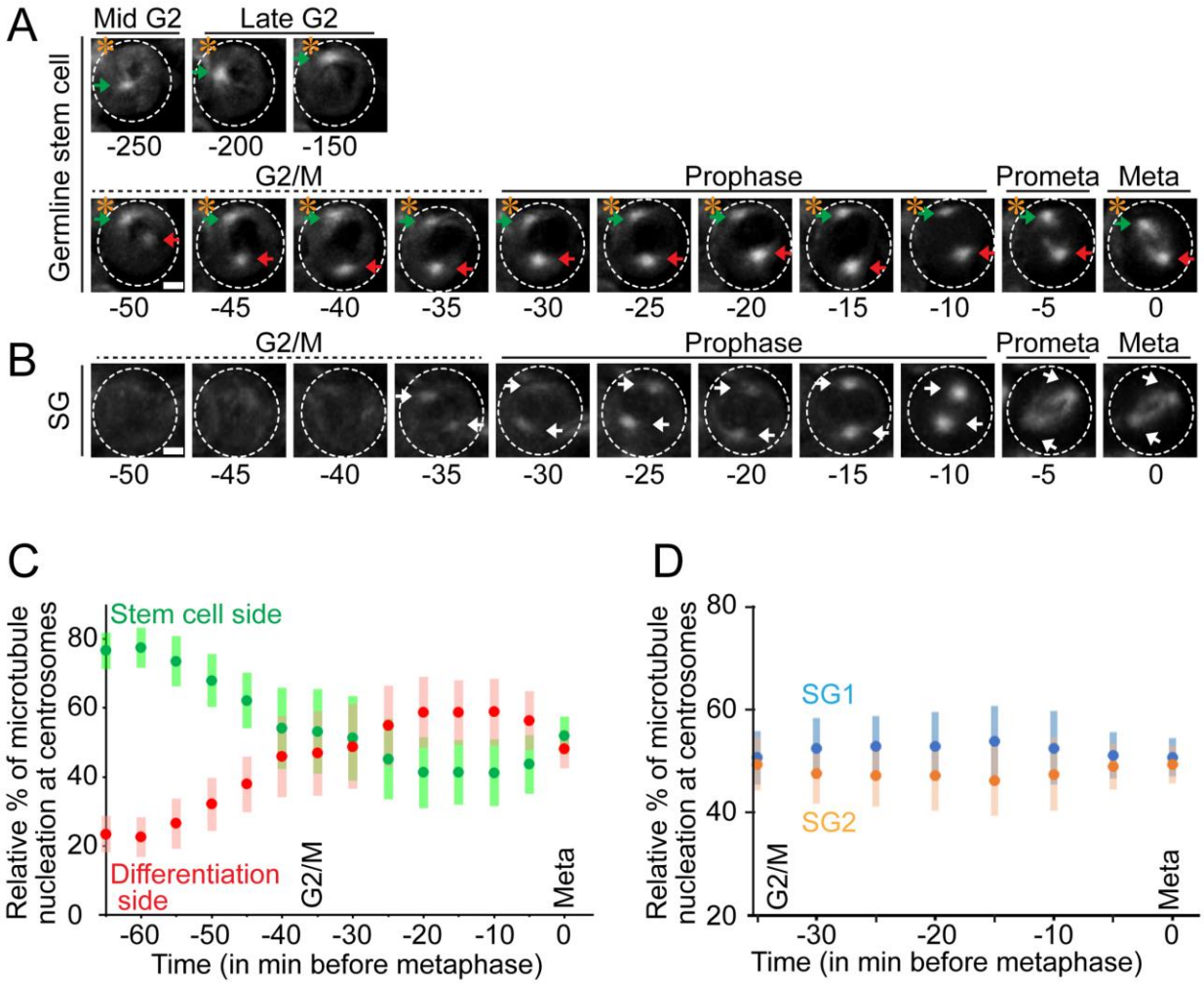

Figure 3: Temporally asymmetric microtubules in GSCs. 3D reconstructed montage made form live cell imaging using a *nanos-Gal4*; *UAS-α-tubulin-GFP* line in GSCs (**A**) and quantified in (**C**, *n*= 22, Table S8), as well as in SGs (**B**) and quantified in (**D**, *n*= 24, Table S8). Metaphase was set as time 0, and other time points prior to metaphase were labeled as minus minutes. (**A**) In GSCs the mother centrosome is activated in mid G2 (- 250 min) prior to the daughter centrosome at G2/M transition (- 50 min). (**B**) In SGs, both centrosomes activate at the G2/M transition (-35 min). (**C**-**D**) All ratios= Avg± SE, see Table S8. Asterisk: hub. Scale bars: 2μm.

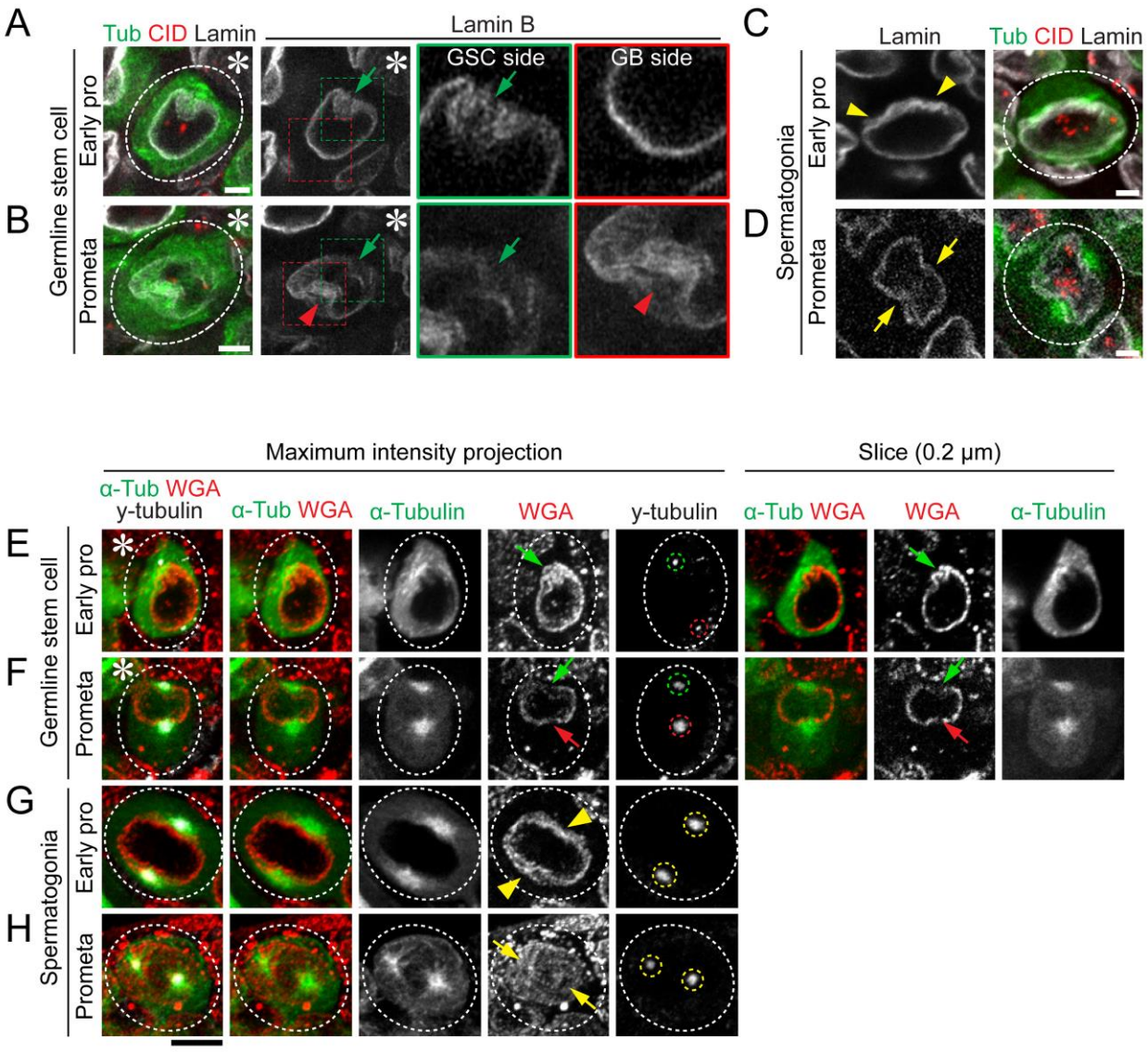

Figure 4: Polarized NEBD in GSCs. (**A**-**B**) Morphology of nuclear envelope in GSCs at early prophase (**A**) and at prometaphase (**B**), as well as in SGs at early prophase (**C**) and at prometaphase (**D**), visualized by immunostaining using anti-Lamin B (white), co-stained with anti-CID (red) using *nanos-Gal4*; *UAS-α-tubulin-GFP* (green) line. Early active mother centrosome- nucleating microtubules correspond with the initial NEBD toward the hub (green arrows in **A** and **B**), whereas later daughter centrosome-nucleating microtubules lead to NEBD toward the other side (red arrowhead in **B**). In contrast, SGs show no polarized NEBD (yellow

arrowheads label invagination sites in **C**, while yellow arrows point to symmetric NEBD sites in **D**). (**E-H**) Morphology of nuclear envelope at different staged GSCs (**E-F**) and SGs (**G-H**), visualized by wheat germ agglutinin (WGA) which binds to the cytoplasmic part of each nuclear pore, co-stained with anti-γ-Tubulin in *nanos-Gal4*; *UAS-α-tubulin-GFP* line. The 'poking in' activities of microtubules were labeled by green arrows (from GSC side) and red arrows (from GB side) in (**E-F**). The interaction between microtubules and nuclear envelope in SGs were shown by yellow arrowheads at 'poking in' sites in (**G**) and yellow arrows at NEBD sites in (**H**). Asterisk: hub. Scale bars: 2 μm.

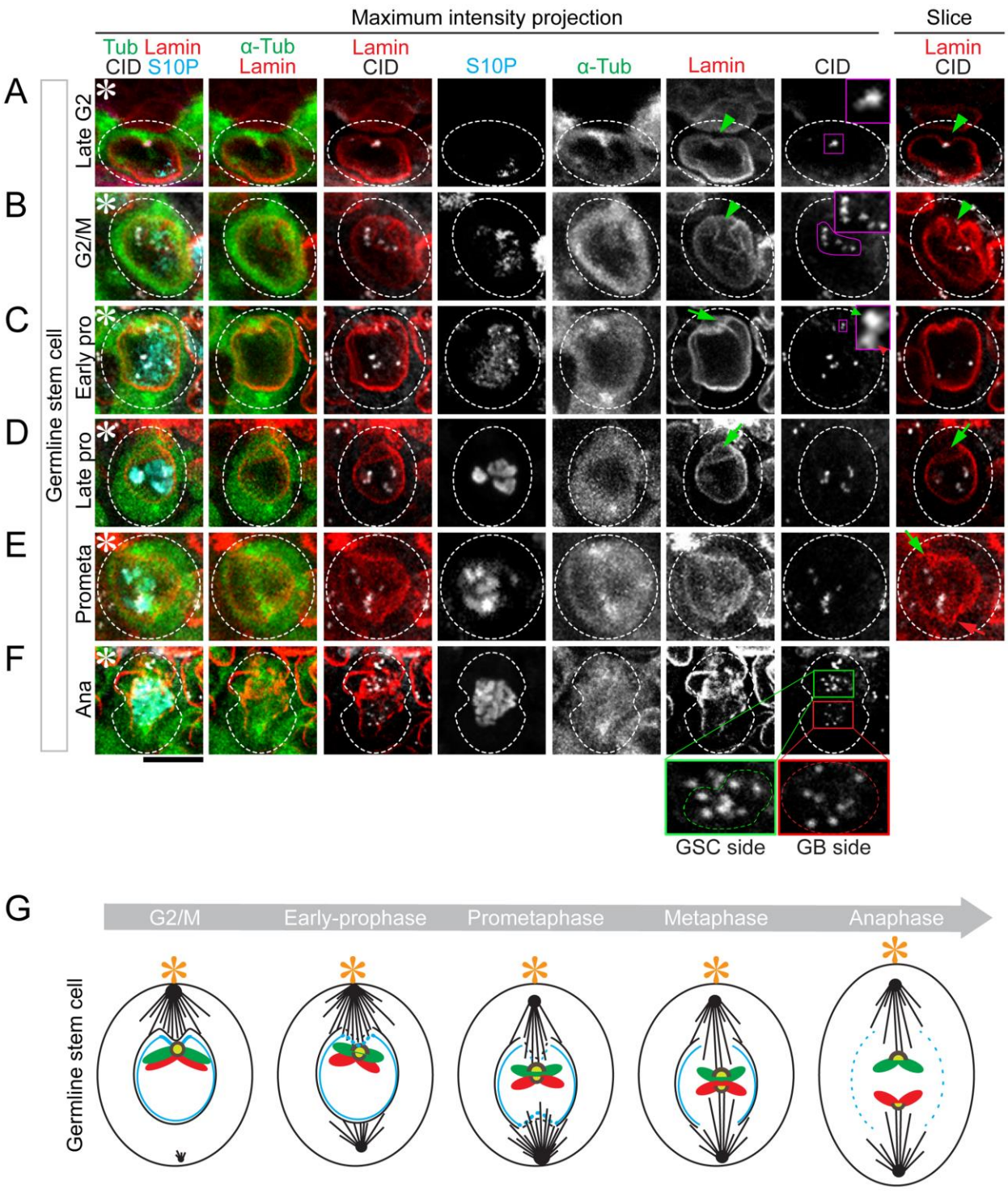

Figure 5: Temporally dynamic microtubules coincide and coordinate with asymmetric sister centromeres. (**A-F**) Morphology of nuclear lamina at different cell cycle stages of GSC, visualized by immunostaining with anti-Lamin B (red), co-stained with anti-CID (white) and

anti-H3S10P (blue) in *nanos-Gal4*; *UAS-α-tubulin-GFP* (green) line. Polarized nuclear lamina invagination and centromere cluster at GSC side was labeled by green arrowheads from late G2 to G2/M transition (**A**-**B**). The 'poking in' activities of microtubules lead to centromere declustering along nuclear membrane (**B**). The 'poking in' activities of microtubules labeled by green arrow (from GSC side) at prophase to prometaphase and red arrow (from GB side) at prometaphase (**C**-**E**). Inset at early prophase show a pair of resolved asymmetric sister centromeres (**C**). (**F**) Inset at anaphase show stronger sister centromeres segregated to the GSC side (green outlines), compared to the sister centromeres segregated to the GB side (red outlines). (**G**) A cartoon depicting the 'mitotic drive' model. Asterisk: hub. Scale bars: 5 μm.

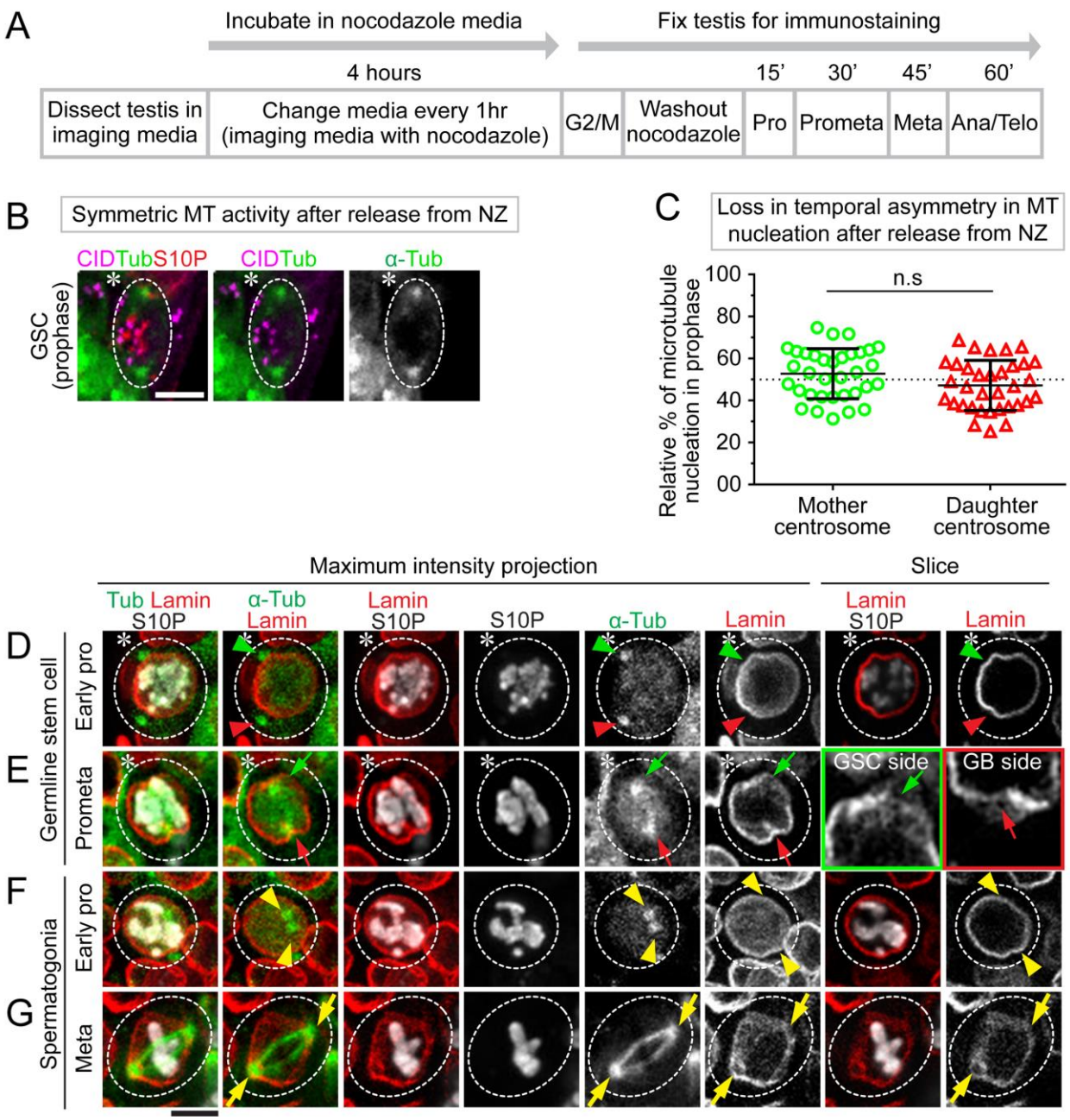

Figure 6: GSCs recovered from Nocodazole (NZ) treatment lose asymmetric microtubule and NEBD. (**A**) A regime of NZ treatment experiment whereby testes were treated with NZ for four hours to arrest GSCs primarily at the G2/M transition. Following washout, GSCs progress into different stages of mitosis in a time-dependent manner. (**B**) Symmetric microtubules nucleate from both centrosomes visualized by α-Tubulin-GFP (green) in GSC after release from

NZ-induced cell cycle arrest. (**C**) Quantification of percentage of microtubules emanated from mother centrosome *versus* microtubules emanated from daughter centrosome in GSCs [52.81± 2.01% from mother centrosome and 47.19± 2.01% from daughter centrosome (*n*= 34), Table S9], showing no significant (n.s) difference by paired *t* test. (**D**-**G**) Morphology of nuclear envelope in GSCs at early prophase (**D**) and at prometaphase (**E**), as well as in SGs at early prophase (**F**) and at metaphase (**G**), visualized by immunostaining using anti-Lamin B (red), co-stained with anti-H3S10P (white) using *nanos-Gal4*; *UAS-α-tubulin-GFP* (green) line. Asterisk: hub. All ratios= Avg± SE; *P*-value in (**C**): paired *t* test. Scale bars: 5 μm.

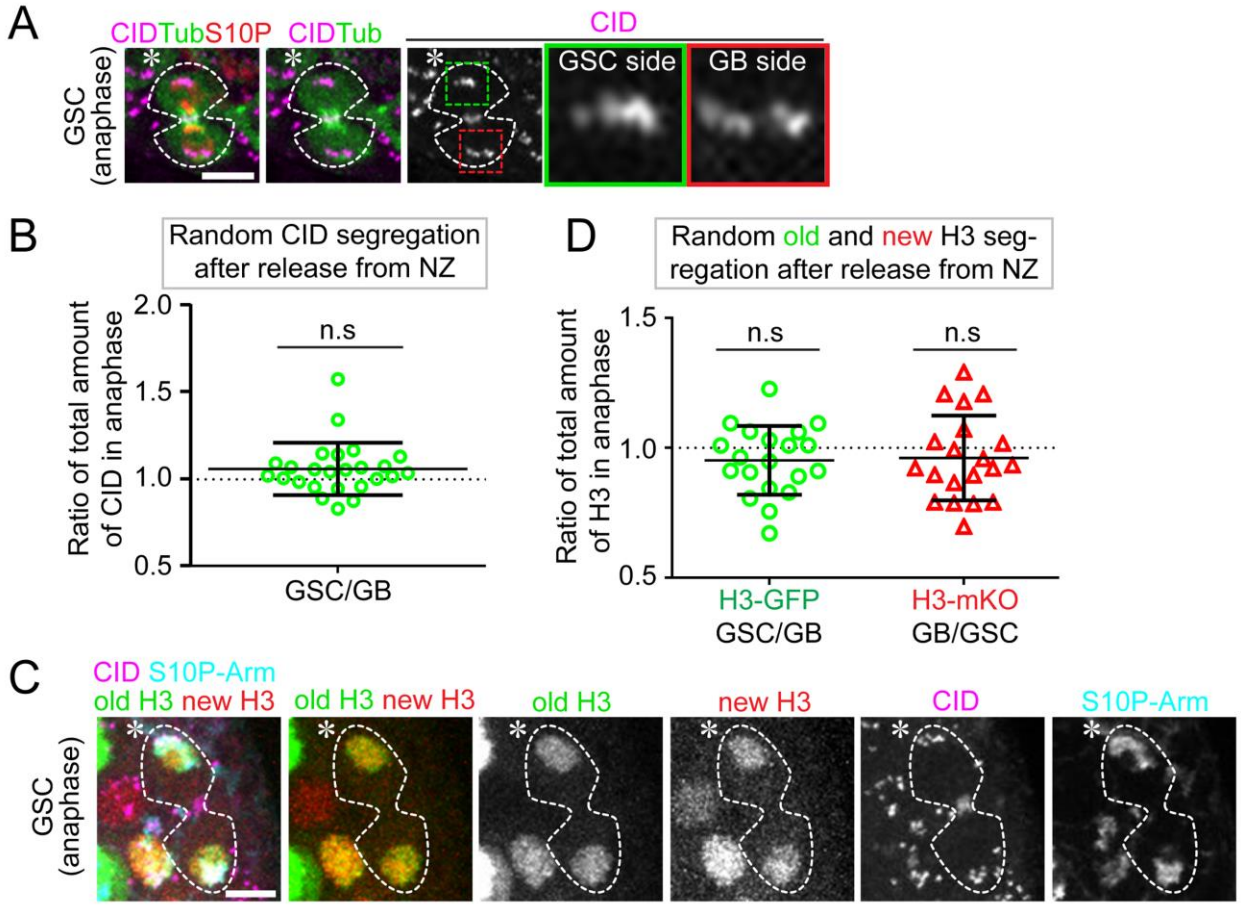

Figure 7: GSCs recovered from NZ treatment display randomized sister chromatid inheritance pattern. (**A-B**) Symmetric CID inheritance pattern in an anaphase GSC after release from NZ-induced cell cycle arrest (**A**), as quantified in [(**B**, 1.06± 0.03-fold, *n*= 25), Table S10]. (**C-D**) Symmetric histone H3 inheritance pattern in an anaphase GSC after release from NZ-induced cell cycle arrest (**C**), as quantified in [(**D**, old H3-GFP GSC/GB= 0.95± 0.03; new H3-mKO GB/GSC= 0.96± 0.04, *n*= 20), Table S11]. Asterisk: hub. All ratios= Avg± SE; *P*-value in (**B**) and (**D**): one-sample *t* test, Scale bars: 5 μm.

References:

Akera, T., Chmatal, L., Trimm, E., Yang, K., Aonbangkhen, C., Chenoweth, D.M., Janke, C., Schultz, R.M., and Lampson, M.A. (2017). Spindle asymmetry drives non-Mendelian chromosome segregation. Science *358*, 668-672.
Allshire, R.C., and Karpen, G.H. (2008). Epigenetic regulation of centromeric chromatin: old dogs, new tricks? Nat Rev Genet *9*, 923-937.
Betschinger, J., and Knoblich, J.A. (2004). Dare to be different: asymmetric cell division in Drosophila, C. elegans and vertebrates. Curr Biol *14*, R674-685.
Cheeseman, I.M. (2014). The kinetochore. Cold Spring Harb Perspect Biol *6*, a015826.
Chen, H., Chen, X., and Zheng, Y. (2013). The Nuclear Lamina Regulates Germline Stem Cell Niche Organization via Modulation of EGFR Signaling. Cell Stem Cell *13*, 73-86.
Chmatal, L., Gabriel, S.I., Mitsainas, G.P., Martinez-Vargas, J., Ventura, J., Searle, J.B., Schultz, R.M., and Lampson, M.A. (2014). Centromere strength provides the cell biological basis for meiotic drive and karyotype evolution in mice. Curr Biol *24*, 2295-2300.
Chudakov, D.M., Lukyanov, S., and Lukyanov, K.A. (2007). Tracking intracellular protein movements using photoswitchable fluorescent proteins PS-CFP2 and Dendra2. Nat Protoc *2*, 2024-2032.
Cleveland, D.W., Mao, Y., and Sullivan, K.F. (2003). Centromeres and kinetochores: from epigenetics to mitotic checkpoint signaling. Cell *112*, 407-421.
Clevers, H. (2005). Stem cells, asymmetric division and cancer. Nat Genet *37*, 1027-1028.
Dawe, R.K., Lowry, E.G., Gent, J.I., Stitzer, M.C., Swentowsky, K.W., Higgins, D.M., Ross-Ibarra, J., Wallace, J.G., Kanizay, L.B., Alabady, M., *et al.* (2018). A Kinesin-14 Motor Activates Neocentromeres to Promote Meiotic Drive in Maize. Cell *173*, 839-850 e818.
Debec, A., and Marcaillou, C. (1997). Structural alterations of the mitotic apparatus induced by the heat shock response in Drosophila cells. Biol Cell *89*, 67-78.
Dunleavy, E., Pidoux, A., and Allshire, R. (2005). Centromeric chromatin makes its mark. Trends in biochemical sciences *30*, 172-175.
Henikoff, S., Ahmad, K., Platero, J.S., and van Steensel, B. (2000). Heterochromatic deposition of centromeric histone H3-like proteins. Proc Natl Acad Sci U S A *97*, 716-721.
Horvath, P., and Barrangou, R. (2010). CRISPR/Cas, the immune system of bacteria and archaea. Science *327*, 167-170.
Hsu, T.C., Cooper, J.E., Mace, M.L., Jr., and Brinkley, B.R. (1971). Arrangement of centromeres in mouse cells. Chromosoma *34*, 73-87.
Inaba, M., and Yamashita, Y.M. (2012). Asymmetric stem cell division: precision for robustness. Cell Stem Cell *11*, 461-469.
Iwata-Otsubo, A., Dawicki-McKenna, J.M., Akera, T., Falk, S.J., Chmatal, L., Yang, K., Sullivan, B.A., Schultz, R.M., Lampson, M.A., and Black, B.E. (2017). Expanded Satellite Repeats Amplify a Discrete CENP-A Nucleosome Assembly Site on Chromosomes that Drive in Female Meiosis. Curr Biol *27*, 2365-2373 e2368.
Jagannathan, M., Cummings, R., and Yamashita, Y.M. (2018). A conserved function for pericentromeric satellite DNA. Elife *7*.
Kahney, E.W., Ranjan, R., Gleason, R.J., and Chen, X. (2018). Symmetry from Asymmetry or Asymmetry from Symmetry? Cold Spring Harb Symp Quant Biol.

Kiseleva, E., Rutherford, S., Cotter, L.M., Allen, T.D., and Goldberg, M.W. (2001). Steps of nuclear pore complex disassembly and reassembly during mitosis in early Drosophila embryos. J Cell Sci *114*, 3607-3618.
Klar, A.J. (1994). A model for specification of the left-right axis in vertebrates. Trends Genet *10*, 392-396.
Klar, A.J. (2007). Lessons learned from studies of fission yeast mating-type switching and silencing. Annu Rev Genet *41*, 213-236.
Kursel, L.E., and Malik, H.S. (2018). The cellular mechanisms and consequences of centromere drive. Curr Opin Cell Biol *52*, 58-65.
Lansdorp, P.M. (2007). Immortal strands? Give me a break. Cell *129*, 1244-1247.
Malik, H.S. (2009). The centromere-drive hypothesis: a simple basis for centromere complexity. Prog Mol Subcell Biol *48*, 33-52.
McKinley, K.L., and Cheeseman, I.M. (2016). The molecular basis for centromere identity and function. Nature reviews Molecular cell biology *17*, 16-29.
Miell, M.D., Fuller, C.J., Guse, A., Barysz, H.M., Downes, A., Owen-Hughes, T., Rappsilber, J., Straight, A.F., and Allshire, R.C. (2013). CENP-A confers a reduction in height on octameric nucleosomes. Nature structural & molecular biology *20*, 763-765.
Morrison, S.J., and Kimble, J. (2006). Asymmetric and symmetric stem-cell divisions in development and cancer. Nature *441*, 1068-1074.
Palmer, D.K., O'Day, K., Wener, M.H., Andrews, B.S., and Margolis, R.L. (1987). A 17-kD centromere protein (CENP-A) copurifies with nucleosome core particles and with histones. J Cell Biol *104*, 805-815.
Pardo-Manuel de Villena, F., and Sapienza, C. (2001a). Female meiosis drives karyotypic evolution in mammals. Genetics *159*, 1179-1189.
Pardo-Manuel de Villena, F., and Sapienza, C. (2001b). Nonrandom segregation during meiosis: the unfairness of females. Mamm Genome *12*, 331-339.
Rieder, C.L. (1981). The structure of the cold-stable kinetochore fiber in metaphase PtK1 cells. Chromosoma *84*, 145-158.
Schroeder, C.M., and Malik, H.S. (2018). Kindr Motors Drive in Meiosis. Cell *173*, 813-815.
Stafstrom, J.P., and Staehelin, L.A. (1984). Dynamics of the nuclear envelope and of nuclear pore complexes during mitosis in the Drosophila embryo. Eur J Cell Biol *34*, 179-189.
Tran, V., Feng, L., and Chen, X. (2013). Asymmetric distribution of histones during Drosophila male germline stem cell asymmetric divisions. Chromosome Res *21*, 255-269.
Tran, V., Lim, C., Xie, J., and Chen, X. (2012). Asymmetric division of Drosophila male germline stem cell shows asymmetric histone distribution. Science *338*, 679-682.
Van Doren, M., Williamson, A.L., and Lehmann, R. (1998). Regulation of zygotic gene expression in Drosophila primordial germ cells. Curr Biol *8*, 243-246.
Westhorpe, F.G., and Straight, A.F. (2014). The Centromere: Epigenetic Control of Chromosome Segregation during Mitosis. Cold Spring Harbor perspectives in biology *7*.
Wooten, M., Nizami, Z.*, Yang, X-X*, Snedeker, J.*, Ranjan, R.*, Kim, J-M., Urban, E., Tran, V., Buss, J., Gall, J., Xiao, J. and Chen, X. (2018). Asymmetric histone incorporation during DNA replication in Drosophila male germline stem cells. bioRxiv 242768 doi:101101/242768
Wright, A.V., Nunez, J.K., and Doudna, J.A. (2016). Biology and Applications of CRISPR Systems: Harnessing Nature's Toolbox for Genome Engineering. Cell *164*, 29-44.

Xie, J., Wooten, M., Tran, V., Chen, B.C., Pozmanter, C., Simbolon, C., Betzig, E., and Chen, X. (2015). Histone H3 Threonine Phosphorylation Regulates Asymmetric Histone Inheritance in the Drosophila Male Germline. Cell *163*, 920-933.
Xie, J., Wooten, M., Tran, V., and Chen, X. (2017). Breaking Symmetry - Asymmetric Histone Inheritance in Stem Cells. Trends Cell Biol *27*, 527-540.
Yadlapalli, S., and Yamashita, Y.M. (2013). Chromosome-specific nonrandom sister chromatid segregation during stem-cell division. Nature *498*, 251-254.
Yamashita, Y.M. (2013). Nonrandom sister chromatid segregation of sex chromosomes in Drosophila male germline stem cells. Chromosome Res *21*, 243-254.
Yamashita, Y.M., Jones, D.L., and Fuller, M.T. (2003). Orientation of asymmetric stem cell division by the APC tumor suppressor and centrosome. Science *301*, 1547-1550.
Yamashita, Y.M., Mahowald, A.P., Perlin, J.R., and Fuller, M.T. (2007). Asymmetric inheritance of mother versus daughter centrosome in stem cell division. Science *315*, 518-521.

Acknowledgements: We thank Y. Yamashita, S. Erhardt, M. Van Doren, R. Johnston and X.C. lab members for insightful suggestions. We thank J. Gall for WGA, S. Erhardt for anti-CID, Johns Hopkins Integrated Imaging Center for confocal imaging. Supported by NIGMS/NIH R01GM112008 and R35GM127075, the Howard Hughes Medical Institute, the David and Lucile Packard Foundation, and Johns Hopkins University startup funds (X.C.).

Author contributions: R.R., J.S. and X.C. conceptualized the study. R.R. and J.S. performed all the experiments and data analysis. R.R. and X.C. wrote the manuscript.

Competing interests: The authors declare no competing interests.

Materials & Correspondence: Correspondence and material requests should be addressed to X.C.

Supplemental Information

Supplemental Experimental Procedures

Fly strains and husbandry

Fly stocks were raised using standard Bloomington medium at 18°C, 25°C, or 29°C as noted. The following fly stocks were used: *hs-flp* on the X chromosome (Bloomington Stock Center BL-26902), *nos-Gal4* on the 2nd chromosome (Van Doren et al., 1998), *UASp-FRT-H3-GFP-PolyA-FRT-H3-mKO* on the 3rd chromosome as reported previously (Tran et al., 2012), *UAS-α-Tubulin-GFP (*Bloomington Stock Center BDSC #7373*)* on the 3rd chromosome and *GFP-cid (*Bloomington Stock Center BDSC #25047*)* on the 2nd chromosome.

Generating knock-in fly strains with key centromere and kinetochore genes tagged

In collaboration with Fungene Inc. (Beijing, China), the following fly lines were generated using the CRISPR-Cas9 technology: CG613329 (*cid*) with Dendra2 tag at the internal site (between 118th - 119th codon), in order to generate the following fusion protein: CID N term-Dendra2-CID C term; CG9938 (*Ndc80*) with Dendra2 tag at the 5' immediately downstream of the START codon, in order to generate the following fusion protein: Dendra2-NDC80.

Heat shock scheme

Flies with *UASp*-dual color histone transgenes were paired with *nos-Gal4* drivers. Flies were raised at 25°C throughout development until adulthood to avoid pre-flip (Tran et al., 2012). Before heat shock, 1-3 day old males were transferred to vials that had been air dried for 24 hours. Vials were submerged underneath water up to the plug in a circulating 37°C water bath

for 90 minutes and recovered in a 29°C incubator for indicated time before dissection for immunostaining experiments.

Immunostaining

Immunofluorescence staining was performed using standard procedures (Hime et al., 1996; Tran et al., 2012). The primary antibodies used were mouse anti-Fas III (1:100, DSHB, 7G10), rabbit anti-Vasa (1:200, Santa Cruz, Cat# sc-30,210), mouse anti α-Spectrin (1:50, DSHB, Cat# 3A9), mouse anti-Armadillo (1;200, DSHB, Cat# N27A1), rat anti-CID (1:200, Active motif, Cat# 61735), rabbit anti-CID (1:200, Active motif, Cat# 69719), mouse anti-Lamin B (1:200, DSHB, Cat# ADL67.10), mouse anti-H3S10P (1:2,000, Abcam, Cat# ab14955), and rabbit anti-H3T3P (1:200, Millipore, Cat# 05-746R). Secondary antibodies were the Alexa Fluor-conjugated series (1:1,000; Molecular Probes). Images were taken using Zeiss LSM 700 confocal microscope, Zeiss LSM 780 confocal microscope, or Zeiss LSM 800 confocal microscope with Airyscan with 63x oil immersion objectives. Airyscan processing was performed to resolve sister centromeres (Figure 1G, 2D-E, 2H, S2E, and S5A), to detect polarized NEBD (Figure 4), and to visualize K-fiber-to-centromere attachment (Figure 1G, S2E, and S5A). Images were processed using Imaris software (3D image reconstruction) and Fiji software (to quantify the total amount of protein "RawIntDen") or to generate maximum intensity projection.

Chromosome spreading

Chromosome spreading was performed to visualize chromosomes and their sister centromeres and sister kinetochores at prometaphase and metaphase. Adult *Drosophila* testes were dissected in Schneider's medium and incubated in a hypotonic solution (0.5% sodium citrate) for 5 minutes

(min) at room temperature (RT). Testes were then fixed in freshly prepared 4 % paraformaldehyde in PBS for 5-7 min at RT on a Superfrost plus slide, a cover slip was placed on top of fixed tissue, and squashed hard. Testes were frozen by immersing them in liquid nitrogen, the cover slip was popped off using a razor blade, followed by immediate incubation in chilled 95% ethanol (-20°C) for 10 min. The immobilized testes were washed three times, 10 min each time, followed by overnight incubation with primary antibodies in blocking solution at 4°C. The testes were then washed three times, 15 min each time, followed by incubation with secondary antibodies for two hours at RT, washed three times, 15 min each time, and mounted in Vectashield without DAPI (Vector, Cat# H-1400).

Live cell imaging

To examine the temporal dynamics of cellular processes during asymmetric GSC divisions, we conducted live cell imaging with high temporal resolution (e.g. 30sec, 60sec or 5min interval as mention in the figure legend and supplemental movie legend). To perform live cell imaging, adult *Drosophila* testes were dissected in a medium containing Schneider's insect medium with 200 µg/ml insulin, 15% (vol/vol) FBS, 0.6x pen/strep, with pH value at approximately 7.0. Testes were then placed on a Poly-D-lysine coated FluoroDish (World Precision Instrument, Inc.), which contains the live cell imaging medium as described above. All movies were taken using spinning disc confocal microscope (Zeiss) equipped with an evolve^{-TM} camera (Photometrics), using a 63x Zeiss objective (1.4 NA). The ZEN 2 software (Zeiss) was used for acquisition with 2x2 binning. Mitotic cells were used to reconstruct 3-D movies using Imaris software (Bitplane). All videos for live cells are shown in Movie S1 – Movie S7.

The 3D quantification for both time-lapse movies and fix images

To quantify the amount of proteins segregated during asymmetric GSC divisions and symmetric SG divisions, we conducted a 3D quantification by measuring the fluorescence signal in each plane from the Z-stack (Figure S1A). The 3D quantification was done at different cell cycle stages (as labeled in the corresponding figures) in GSCs and SGs (e.g. 8-cell cyst), using time lapse movie with *CID-Dendra2* knock-in line, as well as *CID-GFP* and *α-tubulin-GFP* transgenic lines, respectively. The fixed immunostaining images used fluorescence signal of Dendra2 (NDC80), GFP (old histone H3) and mKO (new histone H3), or antibodies recognizing CID. No antibody was added to enhance Dendra2, GFP or mKO signal for quantification.

The 3D quantification of the fluorescence signal was done manually. Un-deconvolved raw images as 2D Z-stacks were saved as un-scaled 16-bit TIF images, and the sum of the gray values of pixels in the image ("RawIntDen") was determined using Fiji (Image J). A circle was drawn to include all fluorescence signal (marked by Dendra2, GFP or mKO), and an identical circle was drawn in the hub region as the background. The gray values of the fluorescence signal pixels for each Z-stack (foreground signal, Fs) was calculated by subtracting the gray values of the background signal pixels (background signal, Bs) from the gray values of the raw signal pixels (raw signal, Rs). The total amount of the fluorescence signal in the nuclei was calculated by adding the gray values of the fluorescence signal from all Z-stacks. The total amount of the fluorescence signal (Fs) in the nuclei with Z-stacks (Z1+…+Zn): Fs (Z1+…+Zn) = [(Rs-Bs)1+…+(Rs-Bs)n].

Nocodazole Treatment

Prior to dissection, Nocodazole (NZ) solution was prepared by adding 1 µl of 2 mg/ml stock solution of NZ in DMSO per 200 µl of imaging media for a final NZ concentration at 10µg/ml.

This solution was left in the dark at room temperature (RT) until needed. Testes were dissected in Schneider's insect media as quickly as possible and transferred to tubes where the excess media was carefully removed. After removing the Schneider's media, 50 µl of NZ solution was added to each tube, which was left open in darkness at RT. Every hour, the old NZ solution was removed and 50 µl of new NZ solution was added for a total of three exchanges or four total hours in NZ solution. At the end of the four hours, the NZ solution was removed and 1 ml of Schneider's insect media was added to each tube except the batch for immediate fixation after NZ, for which 4% formaldehyde was added to the tube instead. For the tubes where NZ was washed out, the media was removed and fresh media was added, repetitively for a total of at least five washes within 15 minutes. Testes were then fixed immediately after washout to catch prophase cells (15 min after release), 30 min after release for prometaphase and metaphase cells, 45 min after release for metaphase and anaphase cells, and 60 to 75 min after release for anaphase and telophase cells (Figure S6A).

Cold treatment to stabilize K-fiber

Adults testes expressing GFP-α-tubulin were dissected and placed into ice cold imaging medium for 5 minutes before fixation and immunostaining using antibodies against CID and H3T3P or H3S10P (Figure 1G, Figures S2E and S5A). Images were collected to visualize the mitotic spindle at metaphase, using the LSM 800 confocal microscope equipped with Airyscan as described above. Images were analyzed to examine orientation of sister centromeres, and their attachment with K-fibers in metaphase GSCs (Figure 1G, Figures S2E and S5A).

Supplementary figures and figure legends:

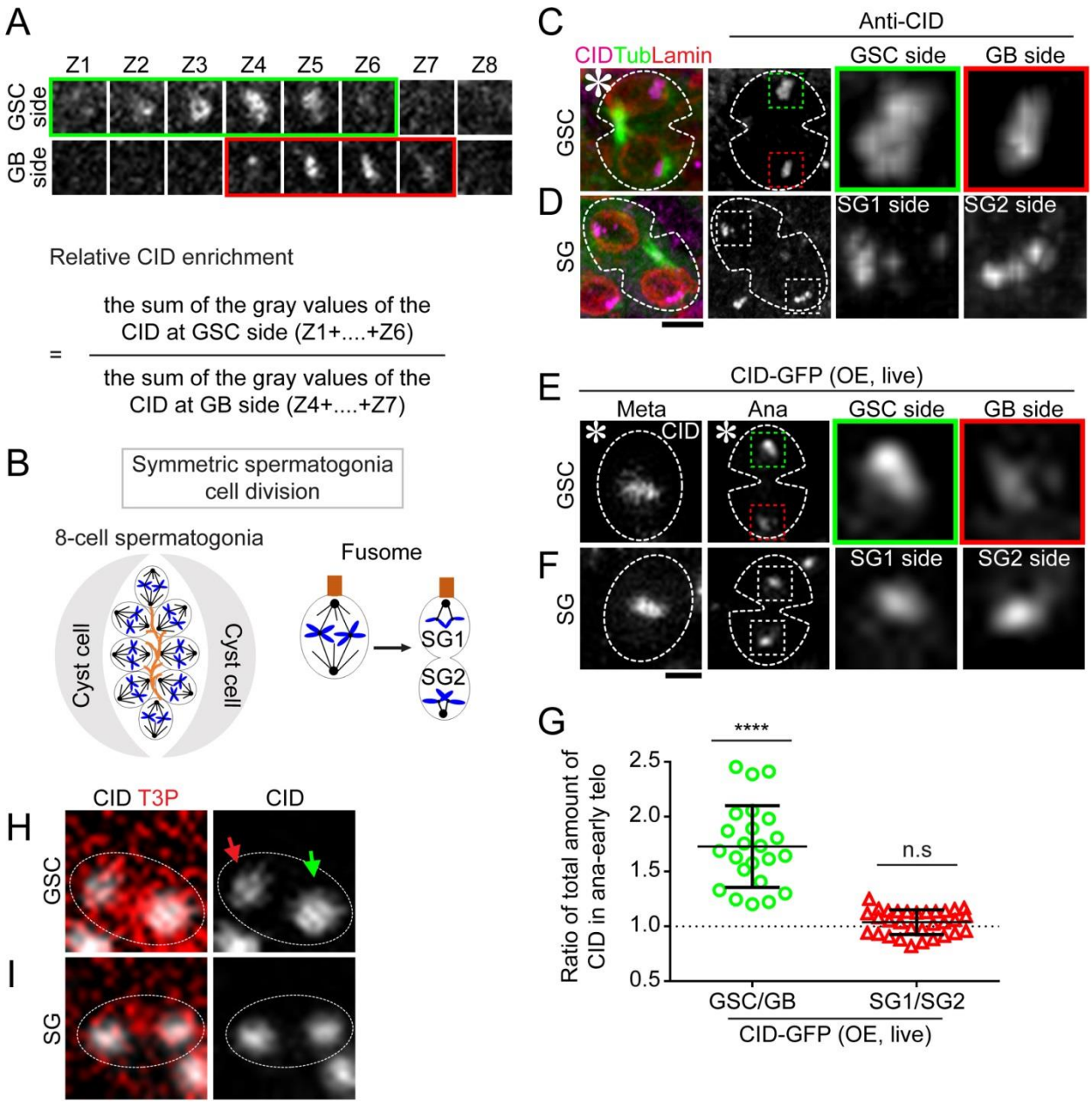

Figure S1: Quantification of CID inheritance pattern in mitotic male germ cells of *Drosophila*. (**A**) Illustration of 3D quantification: total amount of CID toward GSC side or GB side was obtained by summing CID signals from all slices with signals from a Z-stack, with background subtracted from each slice, for example, Z1 through Z6 from the GSC side and Z4 through Z7 from the GB side. The ratio was subsequently deducted by dividing the total amount

of CID from GSC side by the total amount of CID from GB side. (**B**) A cartoon depicting symmetric spermatogonia cell (SG) division. Here SG1 is defined as the one in proximity to the fusome structure while SG2 is the one distal to the fusome. (**C-D**) Images of an early telophase GSC (**C**) and a SG at the same stage (**D**) from *nanos-Gal4*; *UAS-α-tubulin-GFP* testes, immunostained with anti-CID (magenta) and anti-Lamin B (red). (**E-F**) Snapshots from live cell imaging using a *cid-GFP* line, both metaphase and early anaphase were shown for a GSC (**E**) and a SG (**F**). Enlarged images show CID-GFP signals in the anaphase GSC in (**E**) and the anaphase SG in (**F**). (**G**) Quantification of CID-GFP at anaphase or early telophase GSCs and SGs, using method shown in [(**A**), Table S3]. (**H-I**) In prometaphase, resolved individual sister centromeres show more asymmetry in GSCs (**H**), compared with resolved sister centromeres in SGs (**I**). Ratio= Avg± SE; *P*-value: paired *t* test. ****: $P< 10^{-4}$; n.s: no significant difference. Asterisk: hub. Scale bars: 2μm.

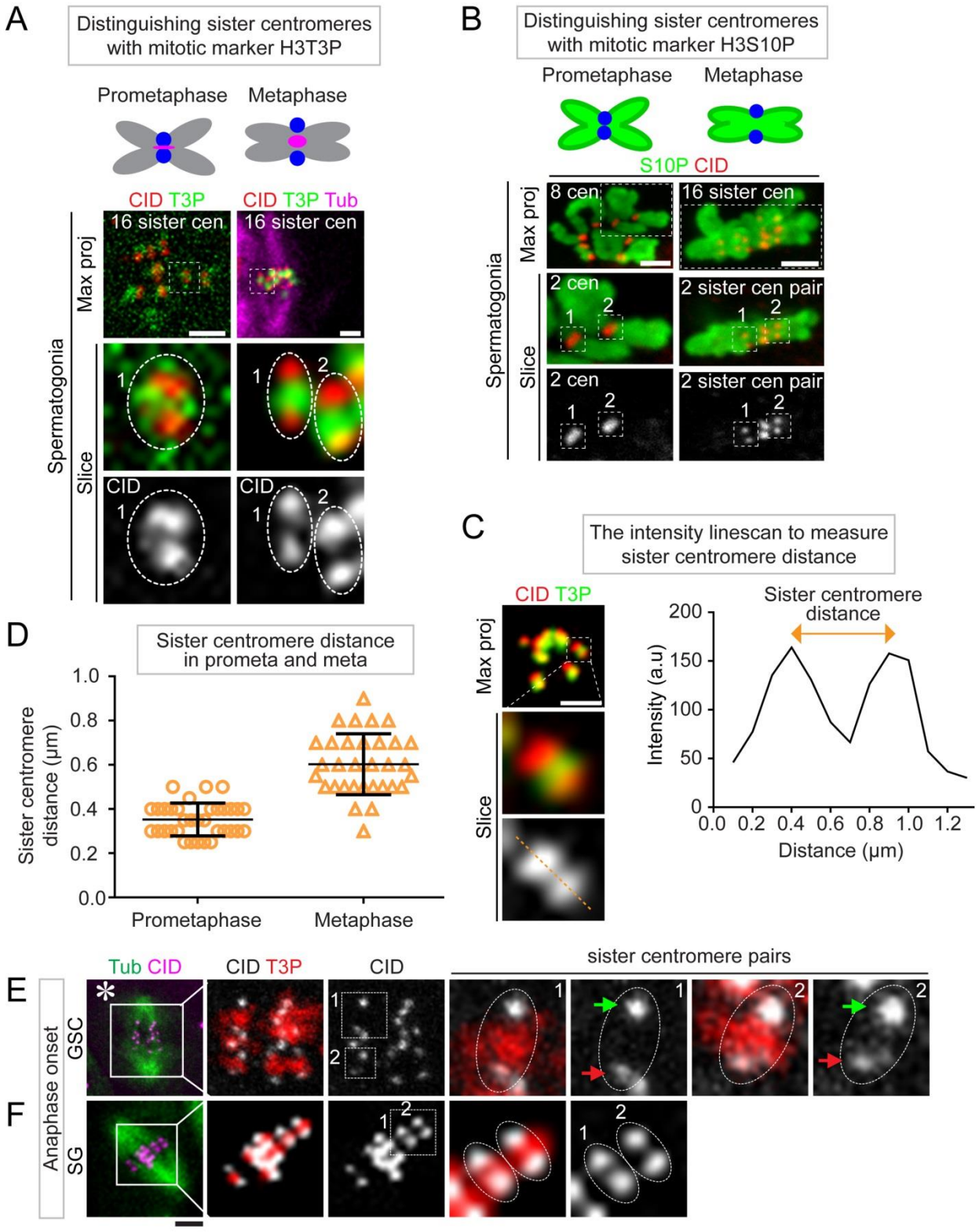

Figure S2: (**A**) A cartoon and examples depict how to use the H3T3P as a cellular mark to distinguish sister centromeres, as used in previous publications (Dai et al., 2005; Lee et al.,

2018). (**B**) A cartoon and examples depict how to use the H3S10P as a cellular mark to distinguish sister centromeres. In these examples, at prometaphase (left side) all eight pairs of sister centromeres (X and Y sex chromosomes, and two of each for the 2^{nd}, 3^{rd}, and 4^{th} autosomes) are visible, shown as eight distinct CID immunostaining signals; while at metaphase (right side), each pair of sister centromeres were resolved into two sister centromere CID signals. (**C**) After determining on sister centromeres, the intensity line scan was performed to measure the distance between sister centromeres. (**D**) At prometaphase, distance between sister centromeres: 0.35$\pm$ 0.01μm; while at metaphase, distance between sister centromeres: 0.60$\pm$ 0.02μm (Table S12). The further resolved sister centromeres were also used as a criterion to distinguish the transition from prometaphase to metaphase, since the moment for all chromosomes aligned as a straight line at the metaphase plate in GSCs could be very transient (compare Figures 1G and S3A in GSCs to Figures 1H and S3B in SGs), necessitating this method to distinguish metaphase GSCs. (**E-F**) At anaphase, the stronger centromere is segregated toward the GSC side (**E**); insets show two asymmetric sister centromere pairs (1 and 2 in **E**). Such phenomenon was not detected in SGs (**F**); insets show two symmetric sister centromere pairs (1 and 2 in **F**). Asterisk: hub. Scale bars: 2μm.

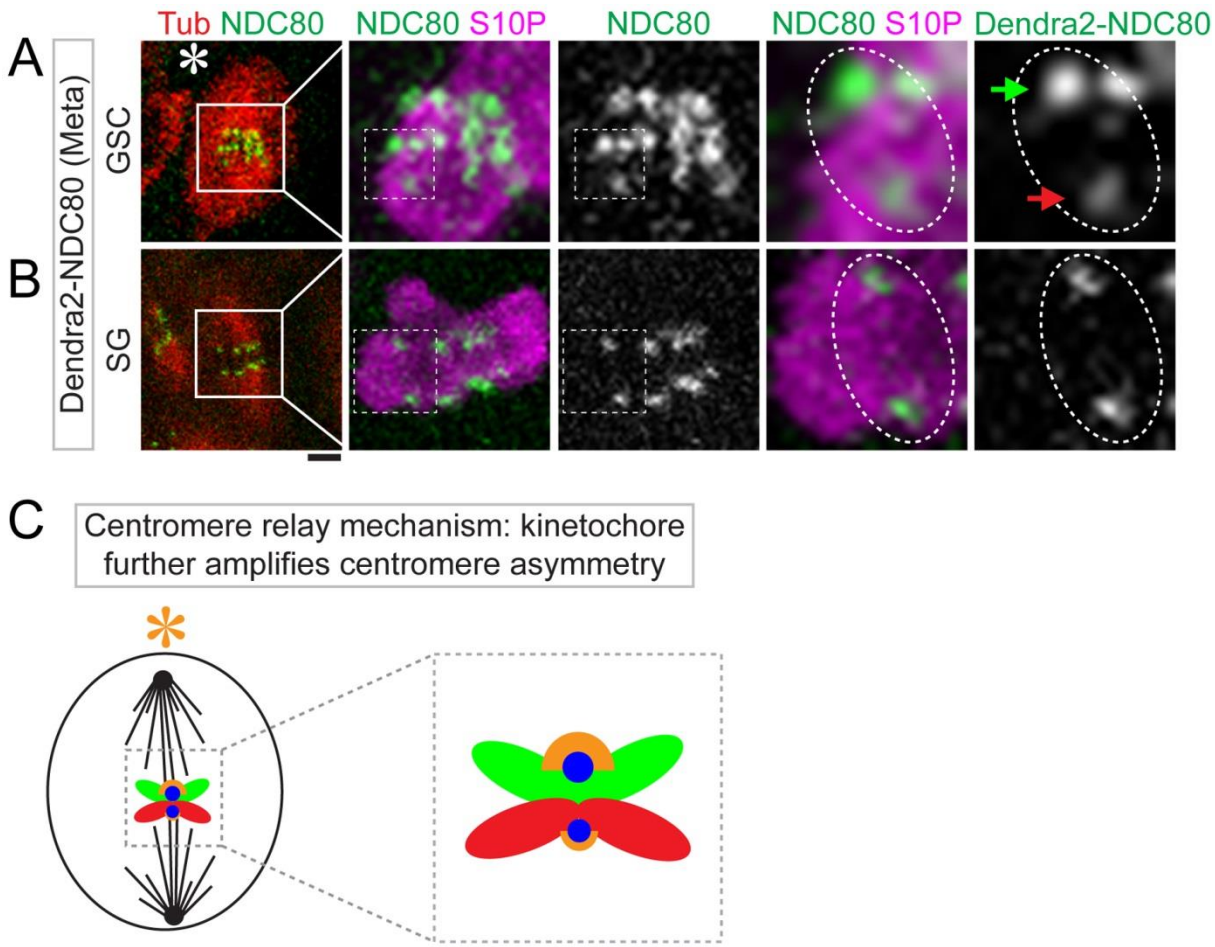

Figure S3: A 'relay' mechanism that transits sister centromere asymmetry to sister kinetochore asymmetry. (**A-B**) At metaphase, the kinetochore component NDC80 showed asymmetry with more signals toward the future GSC side compared to the future GB side between sister kinetochores (**A**). By contrast, symmetric NDC80 was observed between sister kinetochores in SGs (**B**). (**C**) Stronger sister centromeres likely nucleate more kinetochore proteins for attachment by MTs emanated from the stem cell side. Such an asymmetry between sister kinetochores is more than the asymmetry between sister centromeres (Figure 2G, suggesting a potential 'relay' mechanism. Asterisk: hub. Scale bars: 5μm.

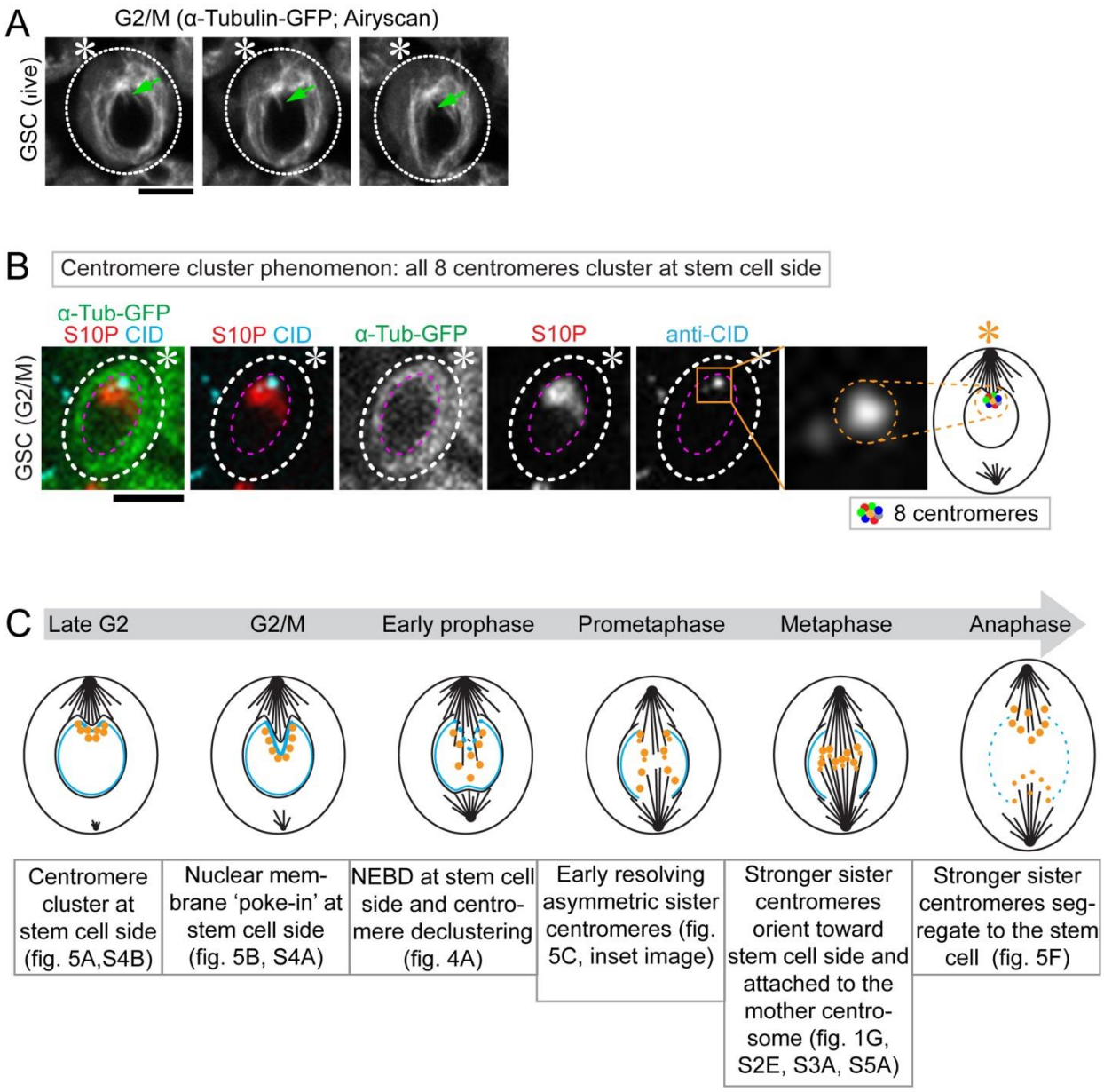

Figure S4: Dynamic interactions between microtubules and centromeres in the mitotic GSCs. (**A**) Snapshots show the 'poking in' activities of microtubules from live cell imaging using the in *nanos-Gal4*; *UAS-α-tubulin-GFP* line (based on Movie S7). (**B**) All CID signals (labeling centromeres from all chromosomes) were clustered near nuclear envelope toward the GSC side in late G2 phase to early prophase. (**C**) A cartoon depicting interaction among

microtubules, nuclear envelope and sister centromeres from late G2 phase throughout mitosis in GSCs. Asterisk: hub. Scale bars: 5μm.

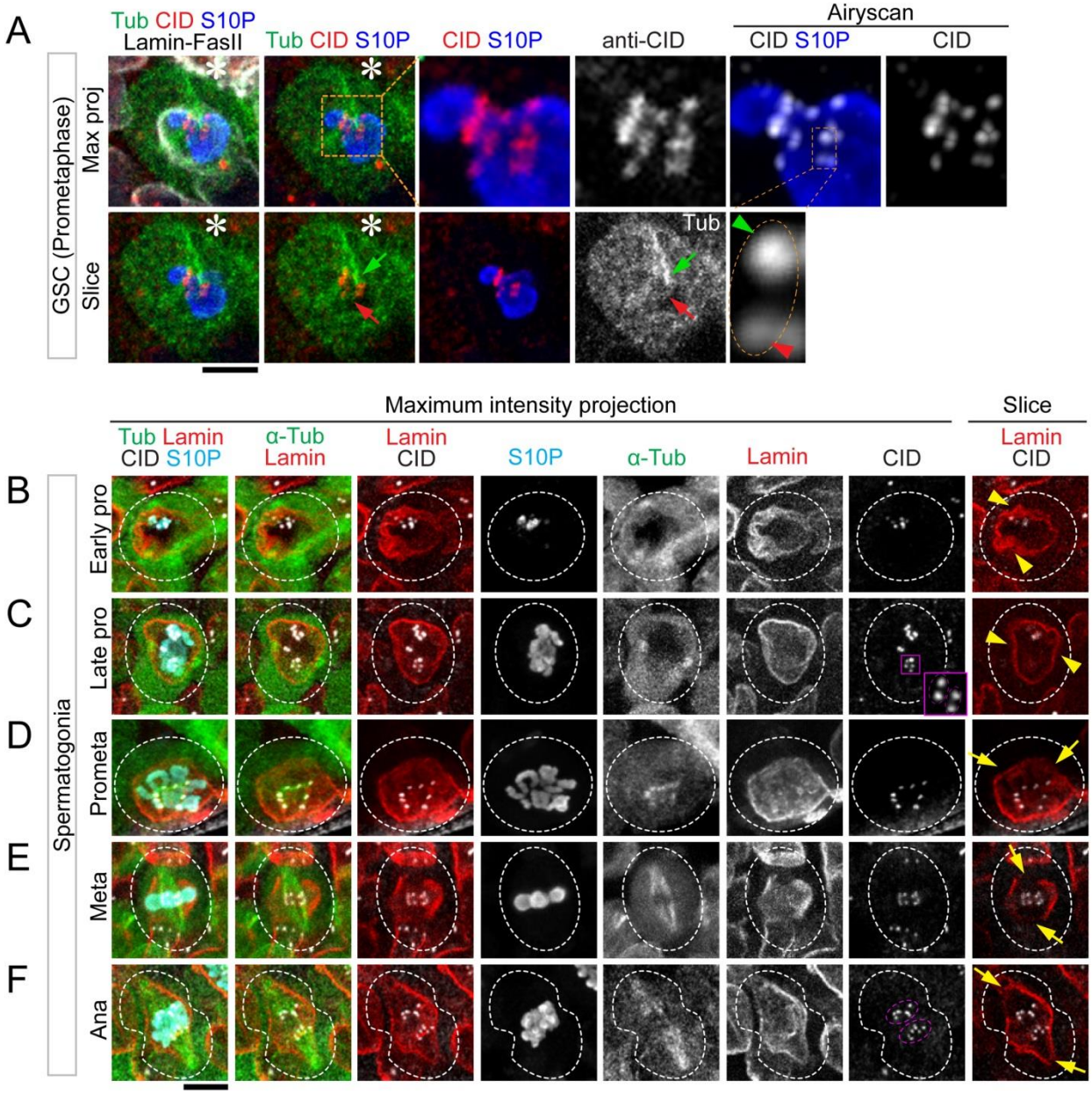

Figure S5: Polarized NEBD potentially allows for differential attachment of microtubules to sister centromeres. (**A**) Stronger sister centromere has more affinity with mother centrosome-emanating K-fibers in GSC at prometaphase. The green arrow points to more K-fibers from the

mother centrosome, and the red arrow indicates fewer K-fibers from the daughter centrosome. Inset images show the asymmetric pair of sister centromeres: the stronger centromere indicated by the green arrowhead (attached by mother centrosome-emanating K-fibers, green arrow) and the weaker centromere indicated by the red arrowhead (attached by daughter centrosome-emanating K-fibers, red arrow). (**B-F**) Morphology of nuclear lamina at different cell cycle stages of SG, visualized by immunostaining with anti-Lamin B (red), co-stained with anti-CID (white) and anti-H3S10P (blue) with the *nanos-Gal4*; *UAS-α-tubulin-GFP* (green) line. Nuclear lamina invagination was detected at both sides in SG labeled by yellow arrowheads at prophase (**B-C**). Inset at late prophase show two pairs of resolved symmetric sister centromeres (**C**). The 'poking in' activities of microtubules were from both poles labeled by yellow arrows at prometaphase (**D**). At anaphase segregated sister centromeres show a symmetric pattern in SG (**F**). Asterisk: hub. Scale bars: 5μm.

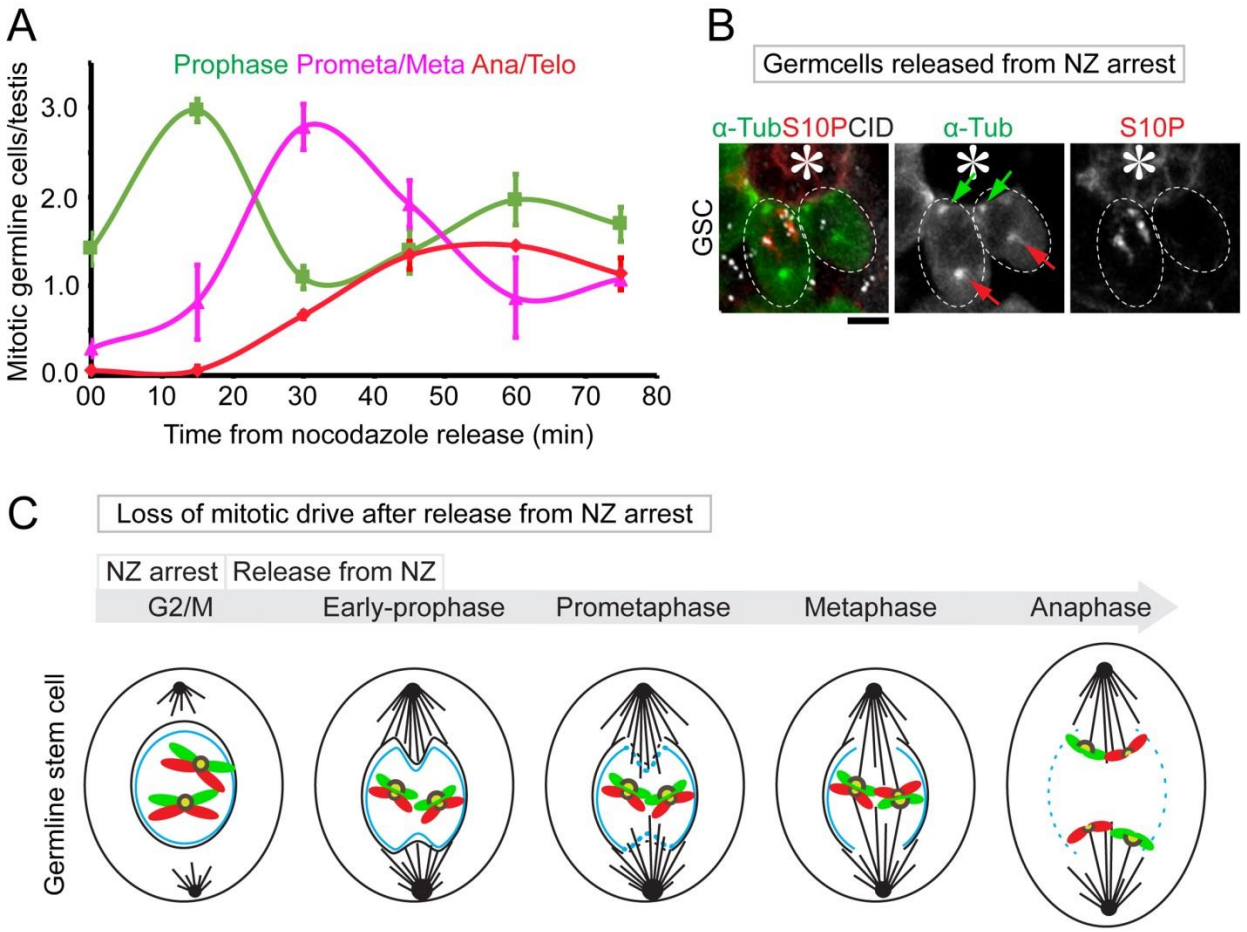

Figure S6: GSCs recovered from Nocodazole (NZ) treatment display time-dependent progression into different stages of mitosis. (**A**) Cells are primarily arrested at G2/M or early prophase immediately following NZ washout, which then progress to prophase after 15 minutes, prometaphase to metaphase after 30 minutes, and anaphase/telophase after 45-60 minutes. All time points = Avg+ SE. (**B**) Symmetric microtubule activity from both centrosomes visualized by α-Tubulin-GFP (green) in GSCs after releasing from NZ-induced cell cycle arrest, co-stained with anti-CID (white) and anti-H3S10P (red). (**C**) A cartoon depicting disruption of the 'mitotic drive' in GSCs recovered from NZ-induced cell cycle arrest, which results in randomized sister centromere segregation as well as randomized old and new histone H3 segregation (see text for detailed discussion). Asterisk: hub. Scale bars: 5μm.

Supplementary movie legends:

Movie S1: Asymmetric CID-Dendra2 segregation in GSC. Live cell imaging of the CID-Dendra2 in a *Drosophila* male GSC: This video is a 3D reconstruction of individual images (8 × 1-μm interval optical sections per frame), showing asymmetric CID-Dendra2 segregation during asymmetric GSC division. The video was acquired at 30sec intervals for 5-6 minutes from prophase to anaphase. Metaphase is used as a landmark to define time point zero, and other time points are labeled as minus minutes prior to metaphase. The quantification is shown in Figure 1D. Asterisk: hub. Scale bar: 2μm.

Movie S2: Symmetric CID-Dendra2 segregation in SG. Live cell imaging of the CID-Dendra2 in a *Drosophila* male SG: This video is a 3D reconstruction of individual images (8 × 1-μm interval optical sections per frame), showing symmetric CID-Dendra2 segregation during symmetric SG division. The video was acquired at 30sec intervals for 5-6 minutes from prophase to anaphase. Metaphase is used as a landmark to define time point zero, and other time points are labeled as minus minutes prior to metaphase. The quantification is shown in Figure 1D. Scale bar: 2μm.

Movie S3: Asymmetric CID-GFP segregation in GSC. Live cell imaging of CID-GFP in a *Drosophila* male GSC: This video is a 3D reconstruction of individual images (8 × 1-μm interval optical sections per frame), showing asymmetric CID-GFP segregation during asymmetric GSC division. The video was acquired at 30sec intervals for 5-6 minutes from prophase to anaphase.

Metaphase is used as a landmark to define time point zero, and other time points are labeled as minus minutes prior to metaphase. The quantification is shown in Figure S1G. Asterisk: hub. Scale bar: 5μm.

Movie S4: Symmetric CID-GFP segregation in SG. Live imaging of the CID-GFP in a *Drosophila* male SG: This video is a 3D reconstruction of individual images (8 × 1-μm interval optical sections per frame), showing symmetric CID-GFP segregation during symmetric SG division. The video was acquired at 30sec intervals for 5-6 minutes from prophase to anaphase. Metaphase is used as a landmark to define time point zero, and other time points are labeled as minus minutes prior to metaphase. The quantification is shown in Figure S1G. Scale bar: 5μm.

Movie S5: Temporal asymmetry of α-Tubulin in GSC. Live cell imaging of α-Tubulin-GFP in a *Drosophila* male GSC: This video is a 3D reconstruction of individual images (14 × 1-μm interval optical sections per frame), showing temporal asymmetry in α-Tubulin-GFP activity at mother centrosome (labeled by green arrow) and daughter centrosome (labeled by red arrow). The mother centrosome is actively nucleating microtubules from mid- to late G2 phase (-240min to -50min), whereas the daughter centrosome nucleates microtubules upon mitotic entry (~ -50 min). Also, in prophase, the dominance of mother centrosome activity becomes less, while microtubules from the daughter centrosome start to increase (-35min to -5min). However, at metaphase microtubules from both sides become equal (0 min). The video was acquired at 5-min interval for 5-6 hrs from mid G2 to G1. Metaphase is used as a landmark to define time

point zero, and other time points are labeled as minus minutes prior to metaphase. The quantification is shown in Figure 3C. Asterisk: hub. Scale bar: 5μm.

Movie S6: Symmetric α-tubulin in SG. Live cell imaging of the α-tubulin-GFP in a *Drosophila* male SG: This video is a 3D reconstruction of individual images (8 × 1-μm interval optical sections per frame), showing neither the mother nor the daughter centrosome nucleates microtubules throughout G2 phase. However, both centrosomes start nucleating microtubules simultaneously upon mitotic entry (~ -35min). The video was acquired at 5-min interval for 5-6 minutes from G2/M to G1. Metaphase is used as a landmark to define time point zero, and other time points are labeled as minus minutes prior to metaphase. The quantification is shown in Figure 3D. Scale bar: 5μm.

Movie S7: A high-resolution time lapse movie of GSC to visualize asymmetric microtubule 'poking in' phenomenon. Live cell imaging of the α-tubulin-GFP in a *Drosophila* male GSC using LSM800 confocal microscopy equipped with Airyscan: This video is a 3D reconstruction of individual images (6 × 0.15μm interval optical sections per frame), showing microtubules spike "poking in" (labeled by green arrow) at GSC side at G2/M transition. The video was acquired at 5-min interval for 30 minutes from G2/M transition to prophase. The G2/M is time point zero; snapshots are shown in Figure S4A. Asterisk: hub. Scale bar: 5μm.

Movie S8: The 3D reconstructed GSC in early-prophase showing NEBD at the GSC side. This video is a 3D reconstruction of individual fixed images (5 × 0.15μm interval optical sections per frame) of α-tubulin-GFP-expressing *Drosophila* male GSC at early prophase, immunostained with anti-Lamin B and anti-CID. (**A**) A 3D reconstruction with α-tubulin-GFP (green), anti-Lamin B (magenta) and anti-CID (red) signals. (**B**) A 3D reconstruction with anti-Lamin B (white) and anti-CID (red) signals. (**C**) A zoom-in view of (**B**). This 3D reconstruction shows asymmetric nuclear envelope breakdown at the GSC side in early prophase. The maximum projection of the image is shown in Figure 4A. Asterisk: hub. Scale bar: 5μm.

Movie S9: The 3D reconstructed GSC in late-prophase showing NEBD at the GSC side and "poking in" phenomenon at the GB side. This video is a 3D reconstruction of individual fixed images (10 × 0.15μm interval optical sections per frame) of α-tubulin-GFP-expressing *Drosophila* male GSC at late-prophase, immunostained with anti-Lamin B and anti-CID. (**A**) A 3D reconstruction with α-tubulin-GFP (green), anti-Lamin B (magenta) and anti-CID (red) signals. (**B**) A 3D reconstruction with anti-Lamin B (white) and anti-CID (red) signals. This image shows that the nuclear envelope at stem cell side is broken, and the nuclear envelope at GB side is "poking in" at late-prophase. The maximum projection of the image is shown in Figure 4B. Asterisk: hub. Scale bar: 5μm.

Supplementary tables and table legends:

Table S1: Quantification of CID in anaphase to early telophase GSCs and SGs by immunostaining using anti-CID.

Pair #	GSC/GB	SG1/SG2
1	1.181852587	1.072688683
2	1.433974059	1.123507204
3	1.755702557	1.142589544
4	1.28693445	1.061786461
5	1.735516044	1.098328681
6	1.262904709	1.010135462
7	1.259372589	1.149435865
8	1.316137585	1.109957322
9	1.227829389	1.086620658
10	1.332531717	0.977108187
11	1.336723733	0.968406269
12	1.304848805	0.974064695
13	1.201435711	1.100481281
14	1.194083643	1.073399858
15	1.20879706	1.045534985
16	1.16374964	0.916112069
17	1.565665091	1.206757464
18	1.258401145	1.058884543
19	1.191521531	0.925785447
20	1.5217	0.910269051
21	1.5701	1.161636493
22	1.587	1.150879872
23	1.531	0.97068742
24	1.686	
25	1.716	
26	1.694	
27	1.551	

Table S2: Quantification of CID-Dendra2 in anaphase to early telophase GSCs and SGs by live cell imaging.

Pair #	GSC/GB	SG1/SG2
1	1.351036022	1.142898421
2	1.151915643	1.18709256
3	1.635341655	1.155233976
4	1.325772996	1.024702142
5	1.243987285	1.022841092
6	1.226437723	1.091847321
7	1.522769663	1.046892536
8	1.335211721	1.004702142
9	1.333865917	1.002841092
10	1.694542979	1.071847321
11	1.616764902	1.026892536
12	1.355781874	0.882695936
13	1.453536058	0.960143503
14	1.244966152	0.942263279
15	1.268494034	0.924058226
16	1.220751075	0.995289367
17	1.413726448	1.108976872
18	1.263630877	1.153306665
19	1.531092331	1.036479976
20	1.531092331	1.058431
210	1.51757744	0.978612
22	1.695118043	
23	1.150776217	

Table S3: Quantification of CID-GFP in anaphase to early telophase GSCs and SGs by live cell imaging.

Pair #	GSC/GB	SG1/SG2
1	1.628534474	1.126563215
2	1.891987337	1.25080379
3	1.870089138	0.855378707
4	2.412713879	0.909605149
5	1.807891532	0.932446439
6	1.616359093	0.820882642
7	1.982243242	1.05901652
8	1.734670914	1.141760345
9	1.517357554	1.137522276
10	2.453457296	0.982201725
11	1.301026153	1.03806825
12	1.577669942	0.941670065
13	1.221849712	0.939137303
14	1.245031491	1.156874829
15	1.407052752	1.140599551
16	1.203254498	1.083258785
17	1.331363218	0.883599481
18	2.055	0.958347113
19	2.387	0.91445709
20	1.756	1.055
210	2.0287	1.1616
22	1.644	1.1686
23	1.689	1.038
24		1.1311
25		1.1204
26		1.025
27		1.136
28		1.0961
29		1.134
30		0.8813
31		0.9719

Table S4: Quantification of sister centromeres in prometaphase GSCs and SGs by immunostaining using anti-CID.

Sister centromere pair #	GSC	SG
1	1.454398955	1.0634278
2	1.581907307	1.3777814
3	2.176156234	1.140667
4	1.741236547	1.0315564
5	1.699125876	1.1013624
6	1.255762531	1.4031346
7	1.351585293	1.052882
8	1.777628993	1.1007956
9	1.704303192	1.1496751
10	1.795453231	1.022172
11	1.421553123	1.0104498
12	1.517118421	1.0231168
13	2.41321584	1.1063371
14	1.821021564	1.1807855
15	1.287924214	1.2682486
16	1.4460641	1.0095048
17	1.522308253	1.095408
18	1.703342201	1.2023619
19	1.548014856	1.4595929
20	1.808520217	1.149548
21	1.538352082	1.1998526
22	1.226093901	1.0630755
23	1.177096933	1.0897182
24	1.838649193	1.2367325
25	1.118389059	1.4739724
26	1.045663473	1.1731339
27	1.823550139	1.0046856
28	1.548014856	1.0534605
29	1.944016052	1.1013694
30	1.517747223	1.2635175
31	1.540362533	1.074951
32	1.375114159	1.103874
33	1.08538421	1.0813608
34	1.056765708	1.33895
35	1.150759142	1.1163995
36	1.912610051	1.0684896
37	1.150454735	1.0339541
38	1.992795765	1.2625603
39	1.5800927	1.1602625

40	1.700652101	1.1922376
41	2.04745014	1.2252916
42	1.978423281	1.2730751
43	1.265846073	1.2643714
44	1.562712458	
45	1.182445488	
46	1.548014856	
47	1.944016052	
48	1.517747223	
49	1.219794276	
50	1.325526552	
51	1.378307066	
52	1.209003771	
53	1.384818529	
54	1.241964123	
55	1.180496206	
56	1.523968091	
57	1.221398675	
58	1.406147701	
59	1.467713081	

Table S5: Quantification of NDC80 in anaphase to early telophase GSCs and SGs using the Dendra2-NDC80 knock-in line.

Pair #	GSC/GB	SG1/SG2
1	1.20591	0.92579
2	1.22725	1.05888
3	1.3778	0.91027
4	1.5641	1.16164
5	1.70618	1.15088
6	1.19781	0.97069
7	1.3176	1.11056
8	1.53487	0.94527
9	1.46742	0.98711
10	1.8596	1.01336
11	1.29055	0.88362
12	1.743	1.01012
13	2.19932	1.16871
14	1.84774	1.15286
15	1.81431	1.08919
16	1.29751	1.32728
17	1.22645	1.02107
18	1.22381	1.13465
19	1.21363	1.17153
20		0.78864
21		0.80937
22		0.97844
23		0.83539
24		1.16991
25		0.99829
26		1.13468
27		0.99595
28		1.02157

Table S6: Quantification of sister kinetochores in prometaphase GSCs and SGs by immunostaining using anti-Dendra2 in Dendra2-NDC80 knock-in line.

Sister kinetochore pair #	GSC	SG
1	1.63255325	1.21391
2	2.08886942	1.45205
3	1.90246077	1.04537
4	1.80469628	1.23229
5	1.34713845	1.15185
6	1.34905403	1.02959
7	1.94231185	1.21227
8	1.23244969	1.10001
9	1.5934456	1.15947
10	1.05108082	1.06496
11	1.69266169	1.1507
12	3.35622859	1.18782
13	2.52883881	1.0143
14	2.51928571	1.04135
15	3.90118243	1.31433
16	1.77010521	1.16524
17	1.558123	1.00982
18	1.24255173	1.19208
19	1.9386881	1.1987
20	1.36099849	1.17504
21	1.44031101	1.21097
22	2.20986391	1.21065
23	1.63049841	1.28595
24	1.64270188	1.15
25	1.50081741	1.64763
26	1.97116416	1.01702
27	2.83562639	1.24521
28	2.10449398	1.14968
29	1.39471604	1.10928
30	1.3243883	1.2998
31	1.21337023	1.19974
32	1.23244969	1.06658
33	1.5934456	1.44734
34	1.25108082	1.36097
35	1.29784861	
36	1.81044933	
37	1.94198314	
38	1.36211499	

39	1.52503629	
40	1.38493551	
41	2.072798	
42	2.58690102	
43	1.37459183	
44	1.67051234	
45	1.24129449	
46	1.34936743	

Table S7: Quantification of sister centromeres using anti-CID and sister kinetochores using anti-Dendra2 in Dendra2-NDC80 knock-in line in prometaphase GSCs.

Sister CID and sister NDC80 Pair #	CID	NDC80
1	1.7	1.9
2	1.84	1.8
3	1.12	1.35
4	1.05	1.35
5	1.82	1.94
6	1.55	1.23
7	1.94	1.59
8	1.52	1.05
9	1.7	1.69
10	1.8	3.36
11	1.54	2.53
12	1.38	2.52
13	1.09	3.9
14	1.06	1.77
15	1.15	1.56
16	1.81	1.24
17	1.54	1.94
18	1.23	1.36
19	1.18	1.44
20	1.91	2.21
21	1.15	1.63
22	1.99	1.64
23	1.58	1.5
24	1.7	1.97
25	2.05	2.84
26	1.98	2.1
27	1.27	1.39
28	1.56	1.32
29	1.18	1.21
30	1.55	1.23
31	1.94	1.59
32	1.52	1.25
33	1.22	1.3
34	1.33	1.81
35	1.38	1.94
36	1.21	1.36
37	1.38	1.53
38	1.24	1.38
39	1.18	2.07

40	1.52	2.59
41	1.22	1.37
42	1.41	1.67
43	1.47	1.24

Table S8: Quantification of microtubules% (of the entire microtubules) from mother centrosome *versus* from daughter centrosome using live cell imaging.

Time in min Before metaphase	GSC (Mother centrosome)	GSC (Daughter centrosome)	SG (centrosome 1)	SG (centrosome 2)
00	51.96 ± 1.16	48.04 ± 1.16	50.73 ± 3.74	49.27 ± 3.74
-05	43.67 ± 1.81	56.33 ± 1.81	51.03 ± 4.51	48.97 ± 4.51
-10	41.2 ± 2.05	58.8 ± 2.05	52.55 ± 7.09	47.45 ± 7.09
-15	41.35 ± 1.99	58.65 ± 1.99	53.88 ± 6.85	46.12 ± 6.85
-20	41.26 ± 2.18	58.74 ± 2.18	52.88 ± 6.72	47.12 ± 6.72
-25	45.2 ± 2.48	54.8 ± 2.48	52.81 ± 6.00	47.19 ± 6.00
-30	51.21 ± 2.61	48.79 ± 2.61	52.49 ± 5.82	47.51 ± 5.82
-35	53.18 ± 2.62	46.82 ± 2.62	50.62 ± 5.19	49.38 ± 5.19
-40	54.08 ± 2.51	45.92 ± 2.51	50.73 ± 3.74	49.27 ± 3.74
-45	62.16 ± 1.71	37.841.71		
-50	67.94 ± 1.64	32.06 ± 1.64		
-55	73.51 ± 1.56	26.491.56		
-60	77.5 ± 1.23	22.51.23		
-65	76.6 ± 1.12	23.41.12		

Table S9: Quantification of microtubules% (of the entire microtubules) from mother centrosome *versus* from daughter centrosome in GSCs after being released from nocodazole treatment using fixed cell imaging.

#	GSC (Mother centrosome)	GSC (Daughter centrosome)
1	50.92747028	49.07252972
2	62.18631017	37.81368983
3	59.28257834	40.71742166
4	42.68494979	57.31505021
5	41.59228266	58.40771734
6	63.39413351	36.60586649
7	47.87278333	52.12721667
8	34.67378808	65.32621192
9	42.45933451	57.54066549
10	56.29206848	43.70793152
11	31.26929056	68.73070944
12	43.56274789	56.43725211
13	64.9450914	35.0549086
14	62.94766542	37.05233458
15	65.45208085	34.54791915
16	36.01826614	63.98173386
17	58.38979391	41.61020609
18	71.73773137	28.26226863
19	71.70944335	28.29055665
20	56.82633109	43.17366891
21	53.53768822	46.46231178
22	35.72544057	64.27455943
23	53.22214387	46.77785613
24	46.53875233	53.46124767
25	62.41700502	37.58299498
26	47.84645406	52.15354594
27	44.81176942	55.18823058
28	74.74046244	25.25953756
29	64.14715064	35.85284936
30	41.80963857	58.19036143
31	34.43054757	65.56945243
32	61.47542203	38.52457797
33	50.28030766	49.71969234
34	60.49091148	39.50908852

Table S10: Quantification of CID signals in anaphase to early telophase GSCs after being released from nocodazole treatment by immunostaining using anti-CID.

Pair #	CID (GSC/GB)
1	0.83121
2	0.95958
3	1.01752
4	1.13137
5	1.57944
6	1.07562
7	1.34462
8	0.88964
9	0.98598
10	1.05838
11	1.02209
12	1.00301
13	1.09289
14	1.14886
15	1.14313
16	0.95585
17	1.16803
18	0.87527
19	1.07041
20	1.00645
21	1.05583
22	1.06752
23	1.04396
24	0.94706
25	1.03688

Table S11: Quantification of old and new H3 after release from nocodazole in anaphase to early telophase GSCs by fixed cell imaging.

Pair #	Old H3 (GSC/GB)	New H3 (GB/GSC)
1	0.80509	0.92097
2	0.84362	0.78429
3	0.90605	0.86517
4	1.09564	0.95767
5	1.00986	1.20735
6	0.7556	1.01741
7	1.09485	1.29103
8	0.94781	0.79019
9	0.67165	0.69703
10	0.91206	1.02308
11	1.01029	1.07116
12	1.0613	0.93353
133	0.96338	1.17816
14	1.03025	0.92203
15	1.06317	1.20747
16	0.82873	0.78745
17	1.0098	0.99231
18	1.22729	0.89431
19	0.91125	0.79001
20	0.89065	0.89638

Table S12: Measurement of the distance between sister centromeres (µm) by immunostaining using anti-CID.

Sister centromere pair #	Prometaphase	Metaphase
1	0.4	0.7
2	0.5	0.7
3	0.3	0.5
4	0.4	0.7
5	0.4	0.8
6	0.5	0.4
7	0.25	0.8
8	0.35	0.6
9	0.3	0.9
10	0.4	0.7
11	0.4	0.6
12	0.3	0.6
13	0.25	0.55
14	0.3	0.6
15	0.35	0.8
16	0.3	0.5
17	0.4	0.5
18	0.3	0.5
19	0.4	0.4
20	0.35	0.5
21	0.4	0.5
22	0.5	0.3
23	0.4	0.6
24	0.4	0.6
25	0.3	0.5
26	0.35	0.8
27	0.3	0.7
28	0.45	0.5
29	0.25	0.7
30	0.3	0.5
31	0.3	0.55
32	0.25	0.7
33	0.25	
34	0.4	

Supplemental References

Dai, J., Sultan, S., Taylor, S.S., and Higgins, J.M. (2005). The kinase haspin is required for mitotic histone H3 Thr 3 phosphorylation and normal metaphase chromosome alignment. Genes Dev *19*, 472-488.

Hime, G.R., Brill, J.A., and Fuller, M.T. (1996). Assembly of ring canals in the male germ line from structural components of the contractile ring. J Cell Sci *109 (Pt 12)*, 2779-2788.

Lee, N.C.O., Kim, J.H., Petrov, N.S., Lee, H.S., Masumoto, H., Earnshaw, W.C., Larionov, V., and Kouprina, N. (2018). Method to Assemble Genomic DNA Fragments or Genes on Human Artificial Chromosome with Regulated Kinetochore Using a Multi-Integrase System. ACS Synth Biol *7*, 63-74.

Tran, V., Lim, C., Xie, J., and Chen, X. (2012). Asymmetric division of Drosophila male germline stem cell shows asymmetric histone distribution. Science *338*, 679-682.

Van Doren, M., Williamson, A.L., and Lehmann, R. (1998). Regulation of zygotic gene expression in Drosophila primordial germ cells. Curr Biol *8*, 243-246.